



Contents lists available at ScienceDirect

Science of the Total Environment

journal homepage: [www.elsevier.com/locate/scitotenv](http://www.elsevier.com/locate/scitotenv)

# Variability of dissolved organic matter in two coastal wetlands along the Changjiang River Estuary: Responses to tidal cycles, seasons, and degradation processes

Xiaohui Zhang<sup>a</sup>, Fang Cao<sup>a</sup>, Ying Huang<sup>a,b</sup>, Jianwu Tang<sup>a,b,c,\*</sup>

<sup>a</sup> State Key Laboratory of Estuarine and Coastal Research, East China Normal University, Shanghai, China

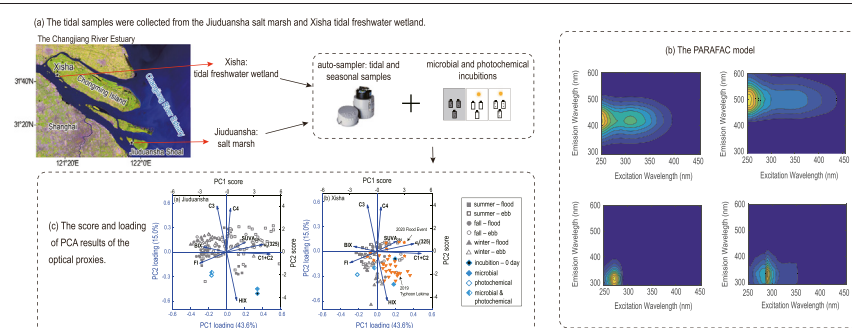
<sup>b</sup> Yangtze Delta Estuarine Wetland Ecosystem Observation and Research Station, Ministry of Education & Shanghai Science and Technology Committee, Shanghai, China

<sup>c</sup> Institute of Eco-Chongming, East China Normal University, Shanghai, China

## HIGHLIGHTS

- The PARAFAC model identified 2 humic-like and 2 protein-like components.
- The quality and quantity of DOM varied on a tidal and seasonal timescale.
- Photochemistry is more effective degrading DOM than microbes in the two wetlands.
- DOM was regulated by both the marsh productivity and the river runoff.
- DOM properties were highly heterogeneous in the coastal wetlands along the CRE.

## GRAPHICAL ABSTRACT



## ARTICLE INFO

### Article history:

Received 2 August 2021

Received in revised form 9 October 2021

Accepted 11 October 2021

Available online xxx

Editor: Jay Gan

### Keywords:

Yangtze River Estuary

Chromophoric dissolved organic matter (CDOM)

Fluorescent dissolved organic matter (FDOM)

Principal component analysis

## ABSTRACT

Dissolved organic matter (DOM) in the coastal tidal marsh–estuary systems are complex mixtures with different source materials that vary with hydrological regimes, seasons, and environmental conditions and are modified by removal processes including photochemical and microbial degradations. Here, monthly surveys of DOM and its optical properties (i.e., absorbance and fluorescence of DOM) covering a complete semi-diurnal tidal cycle were conducted in two coastal marshes with distinct hydrological regimes (i.e., one freshwater and one brackish marsh) in the Changjiang River Estuary (CRE). Four fluorescent components were identified by excitation–emission matrix fluorescence combined with parallel factor analysis (EEMs–PARAFAC) as two terrestrial humic-like components and two autochthonous protein-like components. Results indicated that ebbing waters draining the marshes were consistently enriched with highly absorbing, more humic and highly aromatic DOM compared to the flood tidedwaters. On a seasonal basis, DOM dynamics were largely modulated by the marsh productivity and the seasonal Changjiang runoff. Protein-like fluorophores, however, demonstrated a constant, less variable pattern on both the tidal and seasonal timescales. Onsite water incubation experiments with photochemical and microbial alterations revealed that photochemistry was primarily responsible for the removal of optically active components in the marsh DOM pools whereas the impact of microbes was minor. Principal component analysis (PCA) illustrated the processes regulating the DOM dynamics at the marsh–estuarine interface and allowed a clear distinction of samples between the two marshes, in addition to the samples under the influence of episodic weather events (i.e., Super Typhoon Lekima in summer 2009 and the basin-wide severe flood event occurred in summer 2020). This study underscores the importance of world large-rivers such as Changjiang on estuarine marsh DOM dynamics and also highlights the substantial heterogeneity of the marsh DOM across a river-dominated estuary.

© 2021 Published by Elsevier B.V.

\* Corresponding author at: State Key Laboratory of Estuarine and Coastal Research, East China Normal University, Shanghai, China.  
E-mail address: [jwtang@sklec.ecnu.edu.cn](mailto:jwtang@sklec.ecnu.edu.cn) (J. Tang).

## 1. Introduction

Dissolved organic matter (DOM) is an important component in the global carbon cycle and plays a critical role in a wide range of climate-related biogeochemical processes in aquatic ecosystems, influencing carbon dynamics, nutrient uptake, trace metal cycling, phytoplankton and microbial community structure and function, and ecosystem metabolism, etc. (Benner, 2002; Hedges, 1992). The amount of aquatic DOM represents one of the most abundant active organic carbon reservoirs in the biosphere, which is comparable to the atmospheric CO<sub>2</sub> (Hansell et al., 2009). In the coastal environment, DOM pools are a chemically complex mixture, consisting of allochthonous terrestrial inputs derived from wetlands and riverine runoff, as well as autochthonous materials produced by phytoplankton and detritus (Fellman et al., 2010; Stedmon and Nelson, 2015). Removal processes, such as flocculation (Sholkovitz, 1976), photochemical and microbial degradations (Amon and Benner, 1996; Fasching et al., 2014), significantly modify not only the amount but also the quality (i.e., chemical compositions and molecular structures, etc.) of DOM (Chen and Jaffé, 2014; Logozzo et al., 2021; Lu et al., 2013). Therefore, DOM in the coastal waters often demonstrates seasonal variation in response to these different input and removal processes (Hosen et al., 2018; Osburn et al., 2016). A fraction in the DOM pools is able to absorb sunlight selectively, thereby regulating underwater light climate and subsequently influencing the photo-ecological processes such as primary production and bacterial activities (Arrigo and Brown, 1996; Siegel et al., 2002). These optically active materials are known as chromophoric dissolved organic matter (CDOM). Upon light absorption, a portion in the CDOM pools can subsequently fluoresce. These optical features allow optical approaches to characterize different components in the DOM pools (Coble, 2007; Yamashita and Tanoue, 2003).

Tidal wetland and estuaries along the terrestrial–aquatic margins are hotspots of DOM cycling, where the amount and quality of DOM are modulated by the intense physical and biogeochemical processes which control DOM distribution and transformation, and by the relative contributions of different source materials of DOM (Fagherazzi et al., 2013; Schiebel et al., 2018; Tzortziou et al., 2011). In particular, tidal wetlands are recognized as important carbon sources to coastal waters, roughly contributing up to 35% of total organic carbon input to estuaries along the East Coast of the United States (Herrmann et al., 2015). Indeed, numerous lines of evidence using bulk chemical (Peterson et al., 1994; Wang et al., 2004), optical (Osburn et al., 2015; Tzortziou et al., 2008), and molecular-level (Letourneau and Medeiros, 2019; Lu et al., 2020) analysis indicate that tidal wetlands can be important local sources of DOM to coastal oceans, exporting optically and chemically distinctive materials that are highly absorbing, aromatic-rich and more complex with high molecular weight (HMW) with the ebbing waters to adjacent estuarine systems. These tidal wetland–estuarine systems are also highly vulnerable to natural and anthropogenic perturbations such as episodic weather events, freshwater input (Bittar et al., 2016; Canuel et al., 2012). Hence, accurate understanding of the sources and dynamics of DOM across this critical transition zone

is indispensable for understanding their role in global carbon budgets and interactions with the coastal ocean (Fagherazzi et al., 2013).

Changjiang River, a.k.a. the Yangtze River, runs 6300 m long from the Tibetan Plateau in northwestern China and flows eastward to the East China Sea, draining nearly one-fifth of the mainland area of China. It ranks globally the 4th and 5th largest river in terms of sediment load (e.g.,  $1.05 \times 10^{12}$  kg in 2019) and water discharge (e.g.,  $9.34 \times 10^{12}$  m<sup>3</sup> in 2019) in the world (Milliman and Farnsworth, 2011). Multiple alluvial islands and shoals have been formed along the estuarine salinity gradient (salinity ranges from 0 to ca. 20, A. Gao et al. (2010)) at the Changjiang River Estuary (hereafter referred to as CRE), as a result of the extremely heavy annual sediment loadings. Salt marsh, brackish, and freshwater tidal marsh systems are also developed at the land–estuarine margins, holding important functions in protecting the shoreline from erosion, providing nursery and habitats for breeding and migratory birds (Dai and Lu, 2014; Gan et al., 2009), etc. Previous studies in CRE have mostly focused either on the interannual or seasonal variations of the estuary-wide DOM dynamics (Gao et al., 2020; Liu et al., 2020; Pang et al., 2021; Wang et al., 2012, 2019), or on the DOM changes within tidal creeks along a transect from the marsh to the open waters in CRE (Gao et al., 2011; Tan et al., 2020). Yet, tidal or seasonal variability of DOM at the marsh–estuary interface, or how the marsh DOM can be affected by the degradation processes, particularly for the marshes suited with different salinity regimes in the CRE, have not been investigated.

In this study, monthly surveys of DOM and its optical properties (i.e., CDOM absorbance and fluorescent DOM (FDOM), and their derived optical proxies) covering a complete semi-diurnal tidal cycle, along with onsite incubation experiments were conducted in two coastal marshes with distinct hydrological regimes in the CRE. Our primary focus was to investigate the dynamics of DOM quantity and quality over the short-term (tidal) and long-term (seasonal) timescales, with a particular focus on the discussion of the combined influence of the marsh seasonal cycle and the coincident seasonal runoff from a large river such as Changjiang, on estuarine marsh DOM properties. We employed principal component analysis (PCA) on DOM optical proxies over a broad range of samples collected under different climate scenarios including two episodic weather events (i.e., Typhoon Lekima in summer 2019 and basin-wide flood event across Changjiang in summer 2020), to gain insights on the potential mechanisms driving the DOM dynamics in the two estuarine coastal marshes. Findings from this work advance our understanding of the environmental and ecological controls on modulating DOM dynamics across the tidal marsh–estuarine margins in a large-river-dominated estuary.

## 2. Materials and methods

### 2.1. Sites description

Two coastal marshes, one brackish marsh and one freshwater marsh, suited along the salinity gradient (salinity varied from 0.15 to 18.4 in 2019–2020, Table 1) in the CRE were selected for this study (Fig. 1

**Table 1**  
The hydrological settings in the tidal creeks in JDS and XS marshes during the high and low tides.

Site	Date	Tidal range (m)	Salinity		Temperature (°C)		pH		Turbidity (FNU)	
			H.T. <sup>a</sup>	L.T.	H.T.	L.T.	H.T.	L.T.	H.T.	L.T.
JDS	2019/05/07–2019/05/08	2.3	N.A.	N.A.	N.A.	N.A.	N.A.	N.A.	N.A.	N.A.
	2019/08/30–2019/08/31	3.5	9.01 ± 0.08	0.28 ± 0.49	28.1 ± 0.2	26.4 ± 2.2	7.85 ± 0.05	7.74 ± 0.17	235.3 ± 29.0	130.9 ± 27.7
	2019/11/16–2019/11/17	2.6	10.45 ± 1.23	9.97 ± 0.63	25.2 ± 1.1	22.3 ± 1.6	7.79 ± 0.03	7.48 ± 0.24	237.8 ± 18.2	634 ± 62.8
	2020/01/01–2020/01/02	2.7	10.0 ± 2.1	4.9 ± 1.3	10.6 ± 0.1	10.8 ± 0.1	8.14 ± 0.01	8.08 ± 0.11	143.9 ± 13.2	162.3 ± 4.3
XS	2019/07/15–2019/07/16	2.4	0.23 ± 0.12	0.18 ± 0.03	28.1 ± 0.08	29.9 ± 0.4	7.95 ± 0.03	7.91 ± 0.13	42.0 ± 2.7	29.3 ± 8.5
	2019/09/14–2019/09/15	2.3	0.38 ± 0.01	0.39 ± 0.01	22.8 ± 0.14	20.9 ± 1.5	7.88 ± 0.01	7.57 ± 0.3	166.4 ± 7.2	141.6 ± 7.1
	2019/12/27–2019/12/28	1.2	N.A.	N.A.	N.A.	N.A.	N.A.	N.A.	N.A.	N.A.

<sup>a</sup> H. T.: high tide; L. T.: low tide.

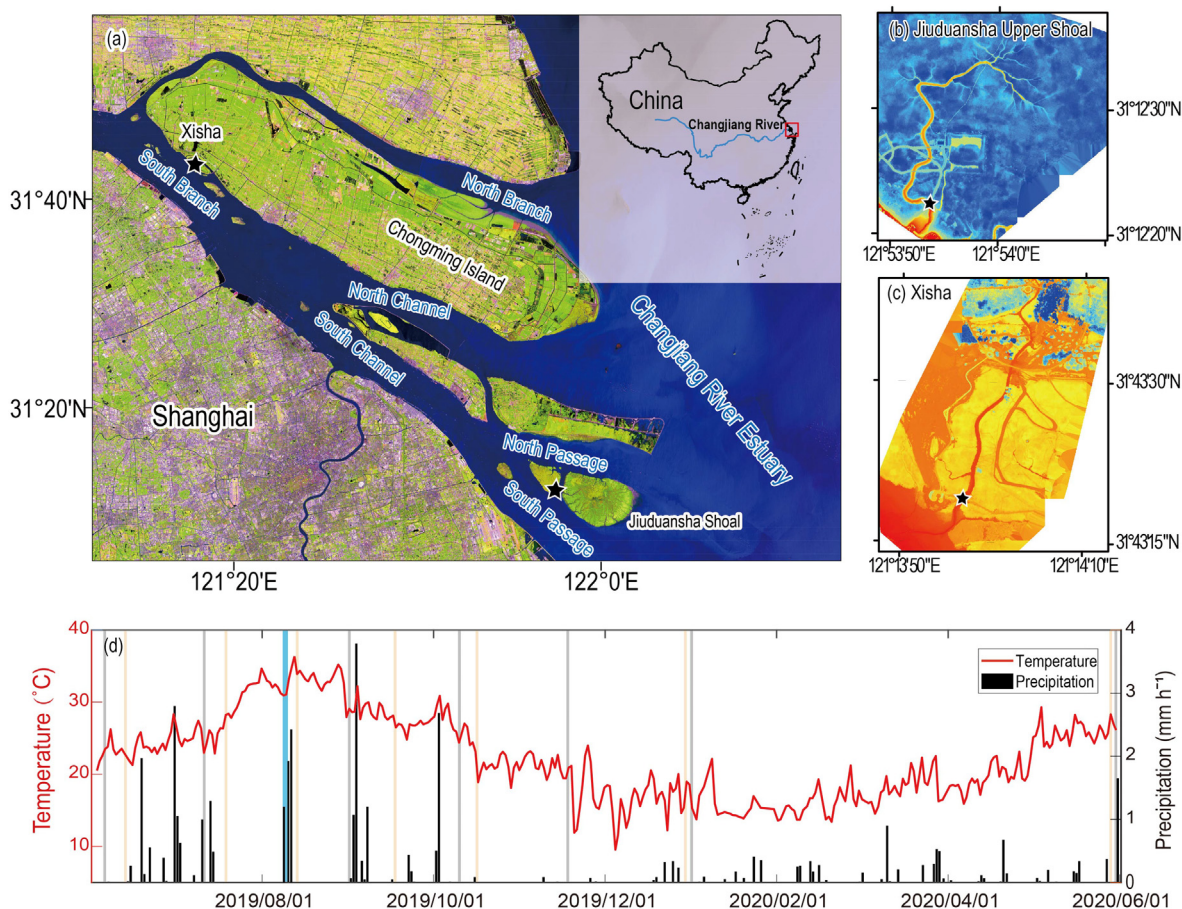


**Fig. 1.** (a–c) Locations of the two study marshes in the Changjiang River Estuary and (d) the temperature and precipitation during May 2019–June 2020. Data sources: (a) Landsat 8 ETM 30 m resolution image (RGB = SWIR 1, NIR, and blue, respectively) acquired on February 29, 2020; (b) and (c) is the digital surface model collected using an unmanned aerial vehicle (Phantom 4 RTK) in May 2021, and the black stars denote the sampling locations. (d) The precipitation and temperature data collected from an eddy covariance tower located in JDS saltmarsh, and the gray and yellow background indicate the sampling time in JDS and XS respectively. The blue background represents the time when Typhoon Lekima passed in August 2019. (For interpretation of the references to color in this figure legend, the reader is referred to the web version of this article.)

(a). The salt marsh study site, encompassing an area of 32.94 km<sup>2</sup>, is located on the Upper Shoal of the Jiuduansha Shoal which is one of the three newly-born isolated alluvial intertidal shoals in the CRE (31°12'22" N, 121°53'53" E, in the Jiuduansha Wetland National Nature Reserve, Fig. 1(b), hereafter referred to as JDS marsh). The Jiuduansha Shoal locates between the South Passage and the North Passage in the estuarine turbidity zone, receiving strong interactions between Changjiang and its adjacent East China Sea. These shoals were initially formed because of the enhanced riverine sediment deposition at the mouth of CRE due to the extreme flood events that occurred frequently during 1949–1954 across the Changjiang River Basin (Li et al., 2016). The freshwater Xisha wetland (31°43'19" N, 121°13'57" E, Fig. 1(c), hereafter referred to as XS marsh) which comprises marsh area of roughly 3 km<sup>2</sup>, is located near the first order bifurcations of Changjiang that are predominately influenced by the riverine discharge (salinity < 0.5 throughout the year). It lies on the western of Chongming Island in Chongming County, in which land use is characterized as rural, agri-ecosystems dominant in northeastern Shanghai, formed before the year of 1842–1860. Hydrology across the two study marshes shows a strong seasonality as a result of precipitation across the Changjiang River basin in response to the East Asian Summer Monsoon, with high discharge during the wet season (May to October) and low runoff in the dry period (November to April) (Fig. 1(d)). The CRE is a meso- to macro-tidal, semidiurnal estuary with a mean tidal range of 2.7 m, whereas the maximum range could rise to 4.7 m during the summertime as a result of the flood season in Changjiang (Yang et al., 2005). Marsh vegetations in the two marshes are dominated by the native

plant species *Phragmites*, while woody plants-*Phragmites* mixed communities, *Phragmites*, and a few *Scirpus-Phragmites* mixed communities are interspersed along the intertidal areas in XS marsh.

## 2.2. Sample collection

Monthly samplings were pursued during spring tide at each of the two marshes from May 2019 to June 2020. Time-series samplings were set up at the inlet of a tidal creek in each marsh, respectively (Table 2). Hourly surface water samples (<0.2 m below surface) covering at least one full tide cycle (24 h) were collected using 1 L polypropylene bottles (acid-soaked in 10% HCl and washed thoroughly using Milli-Q water before use) using an ISCO-7300 Portable Auto-Sampler (Teledyne, CA, USA). After a complete tidal cycle, waters were immediately filtered using a 0.2 μm nylon syringe filter. Filtrates were then collected into 25 mL (pre-combusted at 450 °C for 5 h) amber glass vials and stored at 4 °C for DOM optical analysis within one week. DOC samples were filtered into 20 mL pre-combusted glass vials in the same manner, stored at –20 °C, and analyzed within 1 month. Samples were not obtained occasionally at the lowest ebb tide in the two marshes due to the dry out in marsh tidal creeks in the dry season.

Our monthly sampling also allowed us to capture the DOM changes in response to two episodic weather events, i.e., the passage of the Super Typhoon Lekima in August 2019, and the severe flooding that occurred across the entire Changjiang River Basin in August 2020. Water samples were collected hourly from 4:00 pm to 7:00 pm (GMT + 8) on August 16 and from 3:00 am to 12:00 pm (GMT + 8) on August 17,

**Table 2**  
Sample collection in the two study marshes.

Date	Site	Sampling frequency	Number of samples (N)	Season
Survey samples				
2019/06	JDS	Hourly	26	Summer
2019/07	JDS	Hourly	16	Summer
2019/08	JDS	Hourly	24	Summer
2019/10	JDS	Hourly	20	Fall
2019/11	JDS	Hourly	24	Fall
2020/01	JDS	Hourly	24	Winter
2020/06	JDS	Hourly	28	Summer
2019/06	XS	Hourly	17	Summer
2019/07	XS	Hourly	22	Summer
2019/08 <sup>a</sup>	XS	Hourly	14	Summer
2019/09	XS	Hourly	24	Fall
2019/10	XS	Hourly	17	Fall
2019/12	XS	Hourly	22	Winter
2020/08 <sup>a</sup>	XS	Hourly	23	Summer
Incubation setups				
2020/08	XS	Incubation	12	Summer
2020/08	JDS	Incubation	12	Summer
		Total	325	

<sup>a</sup> Denotes that samples were collected for investigation of the impact of the two extreme weather events (Typhoon event in 2019 and Flood event in 2020).

2019 in XS marsh site (water level less than 1 m). Surveys were also made during the severe flood event in summer 2020, and water samples were collected every hour during ebb tide when the water level gradually retreated from 0.97 to 0.07 m from 10:00 am to 4:00 pm (GMT + 8) on 29 August 2020 in XS marshes. Samplings trips were not attempted to JDS marsh due to the unapproachableness to the Nature Reserve during these two events.

### 2.3. Photo-irradiation and microbial degradation experiments

To assess the impact of photochemical and microbial alterations on DOM, a 5-day incubation experiment was performed onsite in August 2020 in both JDS and XS marshes. Samples were collected at the lowest ebb tide in the two marshes individually and the incubation set-ups consisted of four treatments (i.e., microbial-only degradation, photochemical-only degradation, combined photochemical and microbial degradations, and one control array), with each performed in triplicate (Cao et al., 2016; Medeiros et al., 2015; Seidel et al., 2015). For the photochemical only and combined photochemical and microbial degradation arrays, water samples were filtered using 0.2  $\mu\text{m}$  nylon filters (for photochemical only) or 0.7  $\mu\text{m}$  GF/F filters (for combined photochemical and microbial) and collected into 1 L pre-cleaned polycarbonate bottles and submerged in the water surface under the natural sunlight condition. The irradiance was measured using a HOBO Light Datalogger UA-002-64 sensor (ONSET, USA) during the incubation period. The cumulative 5-day solar irradiance in JDS and XS were 5.4  $\text{kW m}^{-2}$  and 5.7  $\text{kW m}^{-2}$ , respectively. Microbial incubations were carried out in dark by filtering the samples through 0.7  $\mu\text{m}$  GF/F filters (Whatman, pre-combusted at 450  $^{\circ}\text{C}$  for 5 h) into the 1 L pre-cleaned PC bottles, wrapped with a thick layer of aluminum foils in dark plastic bags and kept submerged for 5 days. The control array was set up in a manner similar to the microbial ones but filtering through 0.2  $\mu\text{m}$  nylon filters. The ambient temperatures were maintained at  $24.5 \pm 2.7$   $^{\circ}\text{C}$  for JDS and  $25.1 \pm 1.7$   $^{\circ}\text{C}$  for XS marshes, respectively, during the 5-day incubation experiment.

### 2.4. Laboratory analysis

#### 2.4.1. DOC measurement

DOC concentration was determined using the high-temperature catalytic oxidation method on a Shimadzu TOC-L total organic carbon

analyzer (Tokyo, Japan). Each sample was measured at least three times until the variation coefficient was less than 5%. The linear regression model ( $r > 0.999$ ) of sodium hydrogen phosphate was taken every time to calibrate the analyzer in the concentration gradient of 0, 0.5, 1, 2, and 3  $\text{mg L}^{-1}$ . The deep seawater reference (obtained from D. Hansell Lab, University of Miami, USA, concentration ranged from 0.492 to 0.528  $\text{mg L}^{-1}$ ) was also detected daily for quality control and the reproductivity was better than 97%.

#### 2.4.2. Measurements of DOM optical properties and PARAFAC modeling

Water samples were acclimated to room temperature before optical analysis. CDOM absorbance spectra from 250 to 750 nm with 1 nm intervals were obtained using a UV-visible spectrophotometer UV-8000 (METASH, Shanghai, China) in a 5 cm quartz cuvette using daily produced Milli-Q water as a blank. Absorbance spectra were then corrected for scattering effect by subtracting the mean absorbance value at 700–750 nm (Green and Blough, 1994). CDOM absorption coefficients were then calculated from the corrected absorbance spectra following Eq. (1)

$$a_{\lambda} = 2.303 \times \frac{A_{\lambda}}{L} \quad (1)$$

where  $a_{\lambda}$  ( $\text{m}^{-1}$ ) is the CDOM absorption coefficient at the wavelength  $\lambda$  (nm),  $A_{\lambda}$  is the corrected CDOM absorbance at the wavelength  $\lambda$ , and  $L$  (m) is the path-length of the quartz cuvette and  $L = 0.05$  m in this study. Specific ultraviolet absorbance ( $\text{SUVA}_{254}$ ) ( $\text{L mg}^{-1} \text{m}^{-1}$ ) was calculated by dividing  $a_{\text{g}}(254)$  by the DOC concentration and has been used extensively to denote the DOM aromaticity and molecular weight (Weishaar et al., 2003). CDOM spectral slope coefficients were calculated using a linear fit of a log-linearized  $a_{\lambda}$ , according to Eq. (2)

$$a_{\lambda} = a_{\lambda_0} \times e^{-S(\lambda-\lambda_0)} \quad (2)$$

where  $S$  is the spectral slope range from  $\lambda_0$  to  $\lambda$  (Helms et al., 2008).  $S_{275-295}$  and  $S_{350-400}$  were log-transformed the absorption spectra (subtracting the mean absorbance value at 700–750 nm), then calculated the linear regression slope within the wavelength 275–295 and 350–400, respectively. CDOM spectral slope ratio  $S_R = S_{275-295}/S_{350-400}$  has been used as a tracer of molecular weight of DOM.

DOM fluorescence excitation-emission matrices (EEMs) spectra were collected on a fluorescence spectrophotometer F-4500 (Hitachi, Tokyo, Japan), with daily produced Milli-Q water as a blank. Excitation wavelength (i.e.,  $\lambda_{\text{ex}}$ ) covered from 230 to 455 nm (5 nm increments), and the emission wavelength (i.e.,  $\lambda_{\text{em}}$ ) spanned from 290 to 690 nm (2 nm increments). A 5 nm and 2.5 nm slit widths were adopted in excitation mode and emission mode respectively with a scan rate of 2400  $\text{nm min}^{-1}$ . Several post-processing steps were undertaken to correct the EEMs spectra following EEMs, and included 1) EEM spectra were corrected to remove instrument bias using manufacturer-supplied excitation and emission correction parameters; 2) correction for the inner filter effect (McKnight et al., 2001); 3) blank subtraction using Milli-Q water to remove the water Raman scattering and normalization to the Raman unit using water Raman peak area at  $\lambda_{\text{ex}} = 350$  nm; and 4) Rayleigh and water Raman scatter signals were removed using an interpolation protocol developed by Bahram et al. (2006).

Parallel factor analysis (PARAFAC) was performed on a total of 403 sample EEMs, including 301 field samples and 102 incubation ones, using drEEM 0.5.1 toolbox in MATLAB (MathWorks, MA, USA) (Murphy et al., 2013). Prior to the modeling, sample EEMs were scaled to the unit intensity by dividing the individual fluorescence intensity maxima. Nine samples were identified as outliers and removed, then the model was validated using random split-half analysis. EEMs were

then recovered to the unscaled mode to reflect the actual sample fluorescence intensity for each component.

Fluorescence indices including fluorescence index (FI), humification index (HIX), and biological index (BIX) were calculated to better evaluate the DOM source and compositions. FI is indicative of the organic matter (OM) source materials. Higher FI (~1.8) represents enriched with microbial substances while lower FI (1.2–1.5) reflects terrestrial sourced DOM. FI was calculated as the ratio of fluorescence intensity at  $\lambda_{em} = 450$  nm to  $\lambda_{em} = 450$  nm at  $\lambda_{ex} = 370$  nm (Cory and McKnight, 2005). BIX was calculated by dividing the emission intensity at 380 nm by that in 430 nm with  $\lambda_{ex} = 310$  nm (Huguet et al., 2009). HIX was obtained by calculating the ratio of the peak area under the  $\lambda_{em} = 435$ –480 nm and the sum of peak area under  $\lambda_{em} = 435$ –480 nm and  $\lambda_{em} = 300$ –345 nm, at  $\lambda_{ex} = 254$  nm (Ohno, 2002). HIX and BIX are both indicators of the relative quality of OM from more terrestrial, humic-like OM to more biological, autochthonously produced OM. Specifically, HIX is indicative of the degree of humification and aromaticity of the fluorescent OM and BIX is an indicator of autochthonous, recently produced fluorescent OM in a given sample.

### 2.5. Ancillary data

Ambient water properties including salinity, temperature, pH, turbidity, and fluorescence dissolved organic matter were measured by deploying a pre-calibrated YSI EXO2 multi-parameter Water Quality Sonde (Yellow Springs, OH, USA) at the time of the sample collection. Water levels were measured using a HOBO Water Level Datalogger U20-001-04-Ti sensor (ONSET, USA). Precipitation and air temperature data over the study sites were obtained from an eddy covariance tower at JDS marsh. Daily river flow data was retrieved from the hydrologic station at Datong (Station # 60351, 117°37' E, 30°46' N), which is administrated by the Hydrological Station Changjiang Water Resources Commission of the Ministry of Water Resources (<http://www.cjw.gov.cn/zwzc/gsgg/>) and located approxi. 513 km upstream from the head of CRE.

### 2.6. Statistical analysis

Non-parametric Mann-Whitney *U* test (two-tailed) and Kruskal-Wallis test were performed to evaluate the variations among the samples after performing the normality test using SPSS Statistics 26 (IBM, New York, USA). Principal component analysis (PCA) was conducted for a suite of DOM optical proxies using the relative abundance of fluorescent components and DOM optical properties (e.g., SUVA<sub>254</sub>, FI, HIX, BIX) on the whole dataset from the two marshes including survey and incubation samples. Relative abundance was calculated by log-transforming the absolute values, subtracting the individual means, and dividing by their standard deviations. Variables were checked for collinearity prior to PCA and the highly correlated variables ( $r > 0.8$ ) were combined for subsequent multivariate statistical analysis. The significance level ( $\alpha$ ) was set at 0.05.

## 3. Results

### 3.1. Spectroscopic properties of DOM fluorescence components

PARAFAC modeling on sample EEMs identified and validated four fluorescent DOM components hereafter referred to as C1–C4, including two terrestrial humic-like, two protein-like components (Table 3 and Fig. 2). C1 ( $\lambda_{ex}/\lambda_{em}$ : <260 (310)/418 nm) was assigned as a terrestrially-derived humic component that has widely been observed in sediments, rivers, and estuaries (Brym et al., 2014; Jørgensen et al., 2011; Panettieri et al., 2020). Compared to C1, C2 had a red-shifted emission peak (at ~500 nm), which is indicative of high molecular weight (HMW) DOM with high aromaticity that appears to be prevalent in upstream agriculture regions (Mobed et al., 1996; Yamashita et al., 2011). Fluorescence component C3 demonstrated spectral features ( $\lambda_{ex}/\lambda_{em}$ : 275/316 nm) of a typical protein-like tyrosine material or, peak B, that is often associated with the production from microbial activities in both freshwater and ocean environments (Coble, 2007; Osburn et al., 2018). C4 ( $\lambda_{ex}/\lambda_{em}$ : 290/332 nm) resembled a protein-like tryptophan component. The fluorescence of the amino acid could shift after bounding to protein due to the shielding effect of the water, and C4 was suggested to be the tryptophan amino acid component bonding to protein which emits at shorter wavelengths (Jørgensen et al., 2011; Lakowicz, 2006; Stedmon and Nelson, 2015).

### 3.2. Tidal and seasonal DOM variations

DOM concentration and most of its optical signatures varied as a function of tidal stage and season in the two study marshes. DOC concentration, CDOM absorption coefficient at 325 nm (i.e.,  $a_g(325)$ ) (Fig. 3), fluorescent intensities of humic-like components C1 and C2 were notably higher during low/ebb tide in the summer and fall seasons (e.g., DOC of 3.08 and 3.40 mg L<sup>-1</sup>,  $a_g(325)$  of 5.39 and 4.05 m<sup>-1</sup>, C1 of 0.16 and 0.15 R. U., and C2 of 0.17 and 0.15 R. U. in JDS (water level of 0.14 m) and XS (water level of 0.21 m) marsh in summer 2019, respectively, Fig. 4), indicating the strong marsh export of highly colored, HMW aromatic substances to the adjacent estuary when the marsh productivity peaks (Cawley et al., 2014; Osburn et al., 2015; Tzortziou et al., 2008). Conversely, lower values in DOC,  $a_g(325)$ , and humic components C1 and C3 were consistently found at high/flood tide in the winter season (e.g., DOC of 1.21 mg L<sup>-1</sup>,  $a_g(325)$  of 2.35 m<sup>-1</sup>, C1 of 0.05 R. U., and C2 of 0.04 R. U. in January 2020 (water level of 2.72 m) in JDS marshes). Moreover, C1 and C2 demonstrated a strikingly synchronous pattern in both marshes, suggesting these two components were of a common origin and/or were altered by the same alteration processes (e.g., photochemical or microbial modifications) at nearly identical rates across tidal cycles (Murphy et al., 2008).

Variabilities of protein-like components C3 and C4 however, were dissimilar to most other optical properties but instead, presented no clear pattern on neither tidal nor seasonal scales. For example, C3 and C4 fluctuated in a range of 0.05 R. U. to 0.19 R. U. and from 0.08 R. U. to 0.18 R. U. when the water level dropped monotonously from

**Table 3**  
Spectral characteristics of the five fluorescent components resolved by PARAFAC.

Components	$\lambda_{ex}/\lambda_{em}$ (nm)	Peaks <sup>a</sup>	Description	Compare with previous studies
C1	<260 (310)/418	A/C	Humic acid, derived from terrestrial	C1: 260 (320)/440 (Panettieri et al., 2020) C3: 240 (310)/425 (Brym et al., 2014) C1: 255 (320)/425 (Jørgensen et al., 2011)
C2	240 (320)/500		Humic acid, derived from terrestrial	C2: 260 (420)/498 (Panettieri et al., 2020) C2: 260 (365)/475 (Yamashita et al., 2011)
C3	275/316	B	Tyrosine-like amino acid, microbial activity	C4: 274/322 (Harjung et al., 2018) C5: 270/302 (Osburn et al., 2018)
C4	290/332		Resembling tryptophan-like amino acid	C7: 293/310 (Jørgensen et al., 2011)

<sup>a</sup> The definition of peaks is proposed by Coble (2007).

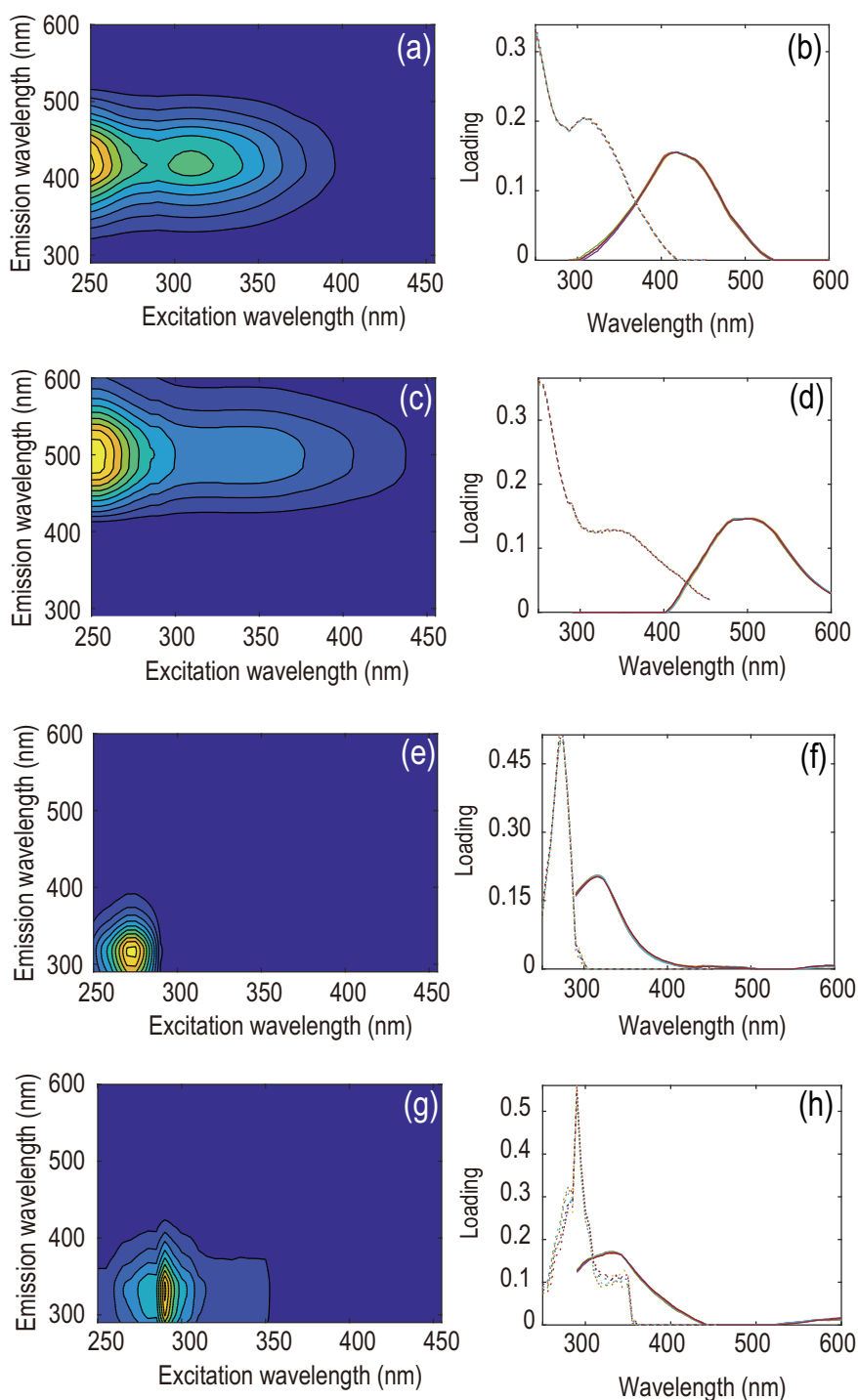


Fig. 2. The spectral features and loadings of fluorescent DOM resolved by the PARAFAC.

3.27 m to 0.27 m (Fig. 4(a)), respectively, likely arose from a diversity of proteinaceous DOM sources materials due to interactions among ecological drivers, hydrological (e.g., physical tidal mixing), and degradation processes on the tidal and season basins.

DOM fluorescence indices also varied widely on both seasonal and tidal time scales, ranging from 1.12 in the summer low tide to 1.76 in high tide in the fall season for FI, from a lowest value of 0.66 in the fall low tide to a highest of 1.29 in the summer high tide for BIX, and from a value of 0.47 at winter high tide to a more elevated value of 0.82 in the low tide in the fall for HIX for JDS marsh, for example (Fig. 5). Elevated FI values which are indicative of more microbially-derived carbon sources are associated with high tide samples during the summer-fall,

while lower values are found with ebbing waters. Notably, winter samples collected demonstrated a converse distribution pattern, with relatively high FI with high tide sample while low FI with high tide in the individual marsh.

### 3.3. Photochemical and microbial alterations on marsh DOM

Results from onsite incubation experiments revealed that photochemistry exerted more pronounced control than microbes on DOM changes in both marshes. CDOM absorption coefficient and humic-like fluorescent intensities of DOM were significantly decreased after the sunlight exposure (e.g.,  $a_g(325) = 2.94 \text{ m}^{-1}$ ,  $C1 = 0.31 \text{ R. U}$ , and

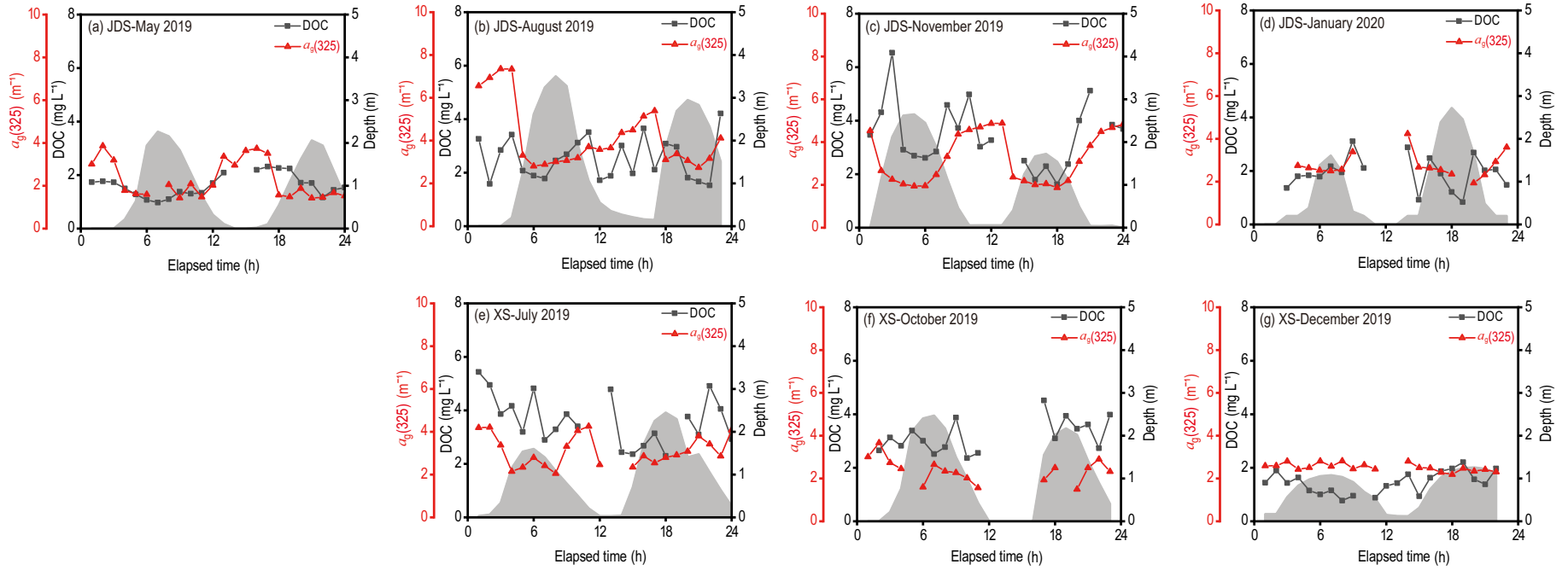


**Fig. 3.** The tidal variation of water level, DOC, and  $\alpha_g(325)$  during a tidal cycle in (a–d) JDS and (e–g) XS marshes, respectively.

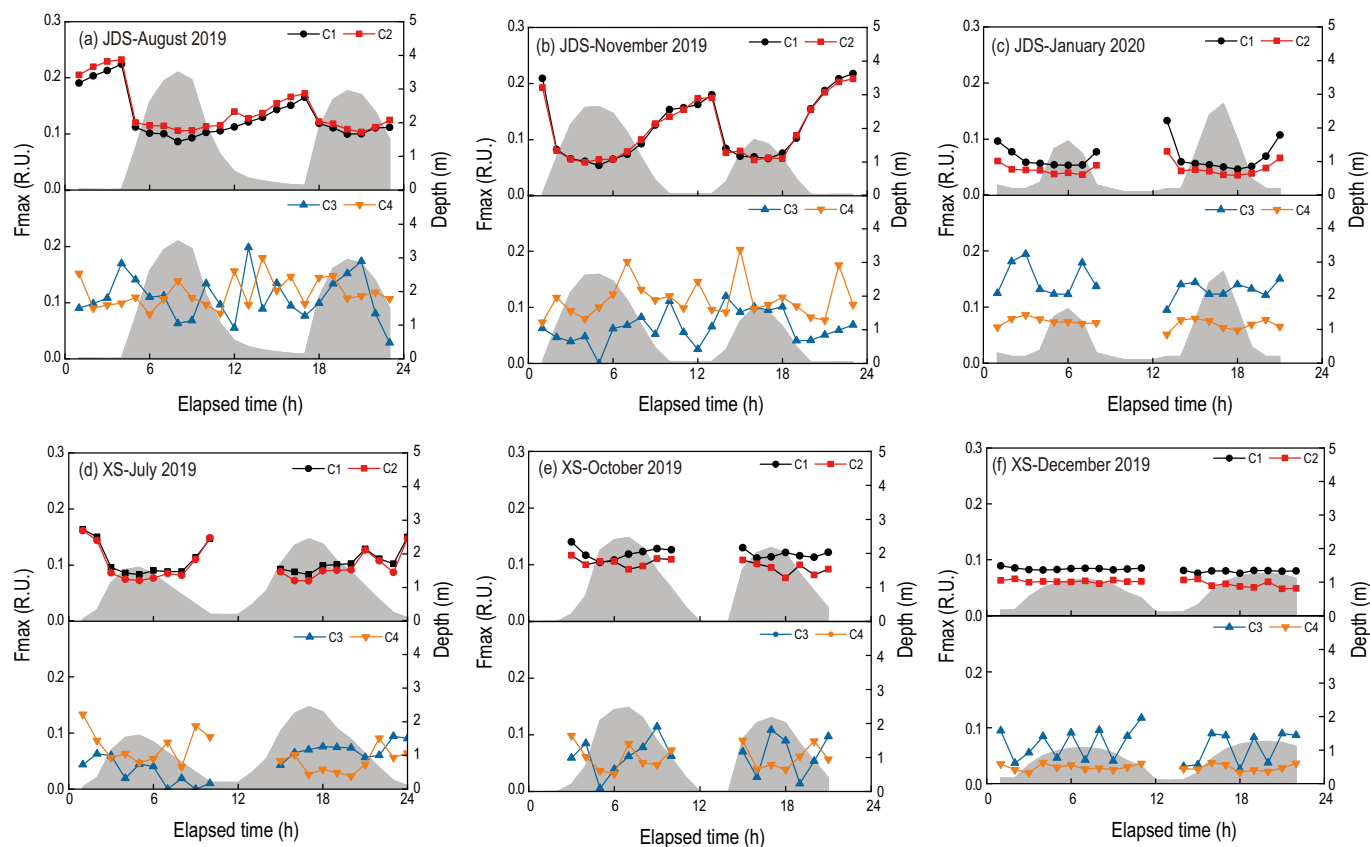


Fig. 4. The tidal variations of the PARAFAC components Fmax in (a–c) JDS and (d–f) XS marshes, respectively.

$C2 = 0.18$  R. U. at  $T = 5$  d, compared to initial values of  $a_g(350) = 4.96$   $m^{-1}$ ,  $C1 = 0.66$  R. U., and  $C2 = 0.41$  R. U. at  $T = 0$  d in JDS marsh, respectively,  $p < 0.05$ ), despite no statistically distinguishable changes in the DOC concentration were identified on neither photochemical (e.g., DOC of  $2.06$   $mg L^{-1}$  at  $T = 5$  d), nor microbial alteration (e.g., DOC of  $2.06$   $mg L^{-1}$  at  $T = 5$  d) over the entire 5-day treatment (e.g., initial DOC of  $2.14$   $mg L^{-1}$  at  $T = 0$  d) (Table 4,  $p > 0.05$ ). The greater decreases in  $a_g(325)$ , accompanied by an increasing  $S_R$ , and the higher loss of fluorescence in humic-like DOM with ebbing water after exposure to sunlight, collectively reflect that marsh-derived, HMW substances were broken down into smaller molecules due to disaggregation and/or ring cleavage, leading to a decrease in the aromaticity ( $SUVA_{254} = 5.65$   $L mg C^{-1} m^{-1}$  at  $T = 5$  d,  $SUVA_{254} = 6.85$   $L mg C^{-1} m^{-1}$  at  $T = 0$  d) (Clark et al., 2019; Helms et al., 2013). On the contrary, dark microbial incubation marginally altered the DOM quality, as revealed by the unchanged values in  $a_g(325)$ ,  $S_R$ , and fluorescence intensities (e.g.,  $a_g(325) = 4.79$   $m^{-1}$ ,  $C1 = 0.70$  R. U., and  $C2 = 0.37$  R. U. at  $T = 5$  d in JDS marsh, respectively,  $p > 0.05$ ), indicating the colored fraction of the marsh DOM pool is largely biologically refractory due to its higher aromaticity and high molecular weight thus less likely available for bacterial utilization in a short 5-day incubation period (Cao et al., 2016; Cory and Kaplan, 2012). The low bioavailability of marsh DOM in this study is also similar to that observed in the marsh in Sacramento-San Joaquin River Delta on the US Pacific Coast (Stepanuskas et al., 2005).

The dominance of the photochemical process in altering marsh DOM is further highlighted by the indiscernible differences between the light-only and the combined light and microbial treatment. Light exposure of marsh DOM with and without the presence of bacteria resulted in a similar percent loss in the CDOM absorption (e.g., ~25% to ~34% decrease in  $a_g(325)$  at  $T = 5$  d in light-only treatment and combined light and microbial treatment) and the humic-like fluorophores (e.g., ~46% reduction in C1 abundance under light-only treatment compared to ~40%

decrease in C1 with combined light and microbial incubation, respectively, in XS marsh for example). These results corroborate previous findings that humic-like fluorophores are more preferentially removed by photochemical modifications in the aquatic systems (Lu et al., 2013; Mann et al., 2012).

#### 3.4. Event-driven DOM changes

Episodic weather events such as tropical cyclones or severe flooding can dramatically alter carbon regimes across the marsh–estuary margins. During our sampling durations, two extreme events, i.e., Super Typhoon Lekima occurred in August 2019 (hereafter referred to as typhoon event), and the severe flood event experienced across the entire Changjiang River Basin due to the monsoon rains in summer 2020 (hereafter referred to as flood event), provide a good opportunity to examine the changes in DOM dynamics in response to these extreme events.

In August 2019, the typhoon event brought continuous precipitation over 167 mm within 60 h to Shanghai area (more details in SI 1). Following this event (~6 days after Typhoon Lekima on 17 August 2019), DOC concentration in XS marsh dramatically increased to a high value of  $6.89$   $mg L^{-1}$  at a water level of 0.3 m. For comparison, DOC concentration collected in July 2019 at a similar tidal height (water level = 0.5 m) was approximately half ( $3.86$   $mg L^{-1}$ ) of that observed during the Typhoon event. Massive flooding as a result of the local heavy precipitation led to the hydrological connection between the coastal marsh and the farmland nearby the marsh via surface flow and/or groundwater (Rudolph et al., 2020). As a consequence, rapid flushing of terrigenous substances from the larger inundated surrounding farmlands and marsh areas gave rise to the elevation in DOC in the ebbing water after the event. This is similar to the DOC pulses noted by Letourneau et al. (2021) in a marsh-dominated estuary after a hurricane event in the southeastern US. Furthermore, the quality of DOM also changed

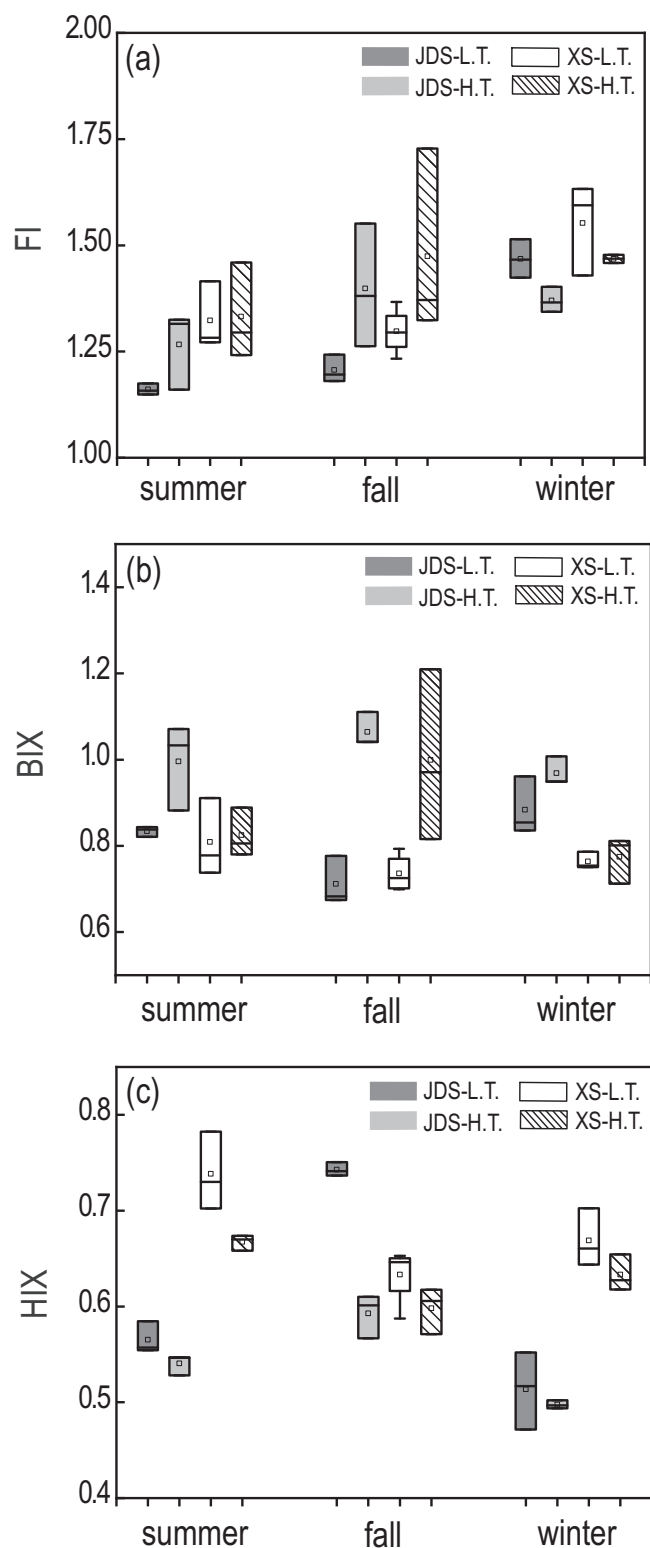


**Fig. 5.** The box plots of (a) FI, (b) BIX, and (c) HIX in JDS and XS marshes, respectively.  
 \*The L.T. and H.T. included the three data at the lowest water level and the highest water level in a tidal cycle, respectively.  
 \*\*The summer, fall, and winter indicated August 2019, November 2019, and January 2020 in JDS, respectively, and July 2019, September 2019, and December 2019 in XS, respectively.

significantly with a decreasing HIX (i.e.,  $HIX = 0.54 \pm 0.07$  (mean  $\pm$  std) after the event, compared to  $HIX = 0.68 \pm 0.03$  in July 2019), accompanied by an increase in  $S_R$  (i.e.,  $S_R = 1.26 \pm 0.03$  after the event,

compared to  $S_R = 1.17 \pm 0.03$ , Kruskal-Wallis test,  $p < 0.005$ ), reflecting a shift of DOM composition from the dominance of allochthonous substances to the pools that were more enriched with autochthonous materials.

In 2020, the summer monsoon season resulted in a historic, basin-wide server flood event in Changjiang. River discharge increased up to  $1.91 \times 10^{12} \text{ m}^3$  at Datong in July 2020, compared to a discharge of  $1.56 \times 10^{12} \text{ m}^3$  in July 2019 (Communique of Yangtze River Water Resources Commission, <http://www.cjw.gov.cn/zwzc/bmgf/2020gb/>). In response to this event, however, we found DOC was only slightly elevated with a value of  $2.97 \text{ mg L}^{-1}$  (water level = 0.7 m) at XS marsh, compared to DOC value of  $2.44 \text{ mg L}^{-1}$  at a similar water stage (water depth = 0.7 m) in July 2019, despite of the 22% increment in Changjiang discharge between these two periods. Yet, significant changes in DOM quality in XS marsh due to the flood event were noted. DOM optical indices show a statistically significant increase in  $SUVA_{254}$  (i.e.,  $SUVA_{254} = 4.68 \pm 0.8 \text{ L mg C}^{-1} \text{ m}^{-1}$  in 2020 summer Flood event, compared to  $SUVA_{254} = 3.34 \pm 0.09 \text{ L mg C}^{-1} \text{ m}^{-1}$  in July 2019) and accordingly decrease in  $S_R$  (i.e.,  $S_R = 0.99 \pm 0.03$ , relative to  $S_R = 1.17 \pm 0.02$  in July 2019), indicating marsh DOM (water level less than 1) was enriched with more aromatic, HMW substances as a result of the flood event.

It is interesting to note that the compositions of DOM changed differently in response to these two episodic weather events and these differences may be in part attributed to the different DOM source materials. In the typhoon event, source materials of DOM flushed to the estuary were not only derived from the wetlands that are often enriched with humic DOM, but also from the nearby forested and restored wood-wetland stream in the supratidal zone, which are often reported to be less complex, low molecular weight, and more enrich in proteinaceous compounds (Bhattacharya and Osburn, 2020). However, during the 2020 Changjiang River basin-wide flood event, Changjiang received tremendous terrigenous inputs from its drainage basin as a large fluvial system, in which landscapes are characterized mainly by forests (38.6%), arable land (29.5%), and grasslands (24.5%) (K. Gao et al., 2010). Many previous studies have shown DOM associated with these land-use types is highly aromatic with dominance of allochthonous contribution (Hosen et al., 2018; Shang et al., 2018). Consequently, with high discharge rates and short residence time, those terrigenous DOM were less modified during transporting to the downstream, resulting in the elevated  $SUVA_{254}$  and lower  $S_R$  observed in DOM in the estuarine coastal marshes during the flood event.

### 3.5. PCA results of DOM optical properties

The multivariate statistical analysis based on DOM optical indices, performed on 254 samples collected for a range of tidal stages across seasons, demonstrates that DOM in flood tide in the summer and fall exhibited distinct optical signatures from those at ebb tide during winter-time in both the two marshes (Fig. 6). Specifically, flood tide samples grouping with negative PC1 scores (ranging from  $-3.69$  to  $-0.02$ ) are largely associated with more recently produced, proteinaceous compounds with elevated BIX (e.g., BIX value as high as 1.25). Whereas the majority of DOM samples collected at ebb tide in the summer–fall seasons that were predominated of allochthonous terrestrial/marsh DOM signatures with higher HIX (e.g., a highest HIX of 0.75 in fall 2019 in JDS marsh), are distributed onto the positive scale in a range of 0.12 to 4.95 on this PC. The clear separation of samples according to the tidal and seasonal shifts on this PC is particularly evident for JDS marsh samples. Most summer and fall ebb tide samples in JDS marsh with a lower BIX (less than 0.82) and small protein-like components contribution of roughly 30–40% in the total fluorescence DOM pools (Fig. 7(a) and (b)) have positive PC1 scores, while the negative scale of PC1 is dominated by the JDS samples collected at the flood stage, in which BIX increased to 1.1 and protein-like components played a more dominant role with relative abundances significantly enhanced

**Table 4**

Results of photochemical-, microbial-, and combined photo-microbial-degradation experiments on the water DOM sampled during the lowest ebb tide in JDS and XS marshes. The incubation duration was 5 days for each treatment.

		Initial condition	Control	Microbial-only	Light-only	Combined light + microbial
JDS	$a_g(254)$ ( $m^{-1}$ )	14.78 ± 0.04 <sup>a</sup>	14.49 ± 0.05	14.39 ± 0.06	<b>12.01 ± 0.2</b>	<b>12.05 ± 0.10</b>
	$a_g(325)$ ( $m^{-1}$ )	4.96 ± 0.01	4.79 ± 0.07	4.80 ± 0.04	<b>2.94 ± 0.10</b>	<b>3.02 ± 0.09</b>
	$S_{275-295}$ ( $nm^{-1}$ )	0.0167 ± 0.0002	0.0166 ± 0.0001	0.0167 ± 0.0002	<b>0.0211 ± 0.0001</b>	<b>0.0209 ± 0.0003</b>
	$S_{350-400}$ ( $nm^{-1}$ )	0.0187 ± 0.0001	0.0191 ± 0.0001	0.0189 ± 0.0001	<b>0.0192 ± 0.0002</b>	0.0188 ± 0.0002
	SR	0.89 ± 0.01	0.87 ± 0.02	0.88 ± 0.01	<b>1.10 ± 0.01</b>	<b>1.10 ± 0.01</b>
	SUVA <sub>254</sub> ( $L\ mg\ C^{-1}\ m^{-1}$ )	6.85 ± 0.11	6.85 ± 0.06	6.79 ± 0.09	<b>5.65 ± 0.12</b>	<b>5.18 ± 0.31</b>
	DOC ( $mg\ L^{-1}$ )	2.14 ± 0.04	2.10 ± 0.02	2.06 ± 0.01	2.06 ± 0.01	2.07 ± 0.03
	C1 (R.U.)	0.66 ± 0.03	0.68 ± 0.03	0.71 ± 0.03	<b>0.31 ± 0.01</b>	<b>0.31 ± 0.01</b>
	C2 (R.U.)	0.41 ± 0.01	0.40 ± 0.01	0.37 ± 0.07	<b>0.18 ± 0.01</b>	<b>0.18 ± 0.01</b>
	C3 (R.U.)	0.02 ± 0.01	0.03 ± 0.01	<b>0.03 ± 0.001</b>	0.04 ± 0.01	<b>0.04 ± 0.02</b>
	C4 (R.U.)	0.11 ± 0.001	0.13 ± 0.02	0.14 ± 0.01	<b>0.17 ± 0.02</b>	<b>0.22 ± 0.01</b>
XS	$a_g(254)$ ( $m^{-1}$ )	13.19 ± 0.01	12.98 ± 0.04	13.22 ± 0.08	<b>11.13 ± 0.04</b>	<b>11.92 ± 0.06</b>
	$a_g(325)$ ( $m^{-1}$ )	4.27 ± 0.01	4.14 ± 0.03	4.26 ± 0.02	<b>2.83 ± 0.04</b>	<b>3.21 ± 0.04</b>
	$S_{275-295}$ ( $nm^{-1}$ )	0.0169 ± 0.0002	0.0172 ± 0.0001	0.0170 ± 0.0001	<b>0.0203 ± 0.0001</b>	<b>0.0199 ± 0.0001</b>
	$S_{350-400}$ ( $nm^{-1}$ )	0.0184 ± 0.0002	0.0184 ± 0.0002	0.0179 ± 0.0001	0.0181 ± 0.0001	<b>0.0172 ± 0.0001</b>
	SR	0.95 ± 0.01	0.93 ± 0.01	0.95 ± 0.01	<b>1.12 ± 0.01</b>	<b>1.15 ± 0.01</b>
	SUVA <sub>254</sub> ( $L\ mg\ C^{-1}\ m^{-1}$ )	5.31 ± 0.06	5.22 ± 0.05	4.93 ± 0.41	<b>4.30 ± 0.03</b>	<b>4.56 ± 0.10</b>
	DOC ( $mg\ L^{-1}$ )	2.46 ± 0.20	2.66 ± 0.16	2.77 ± 0.21	2.67 ± 0.13	2.59 ± 0.05
	C1 (R.U.)	0.61 ± 0.05	0.54 ± 0.08	0.52 ± 0.01	<b>0.33 ± 0.01</b>	<b>0.37 ± 0.01</b>
	C2 (R.U.)	0.31 ± 0.01	0.32 ± 0.001	0.31 ± 0.01	<b>0.21 ± 0.02</b>	<b>0.27 ± 0.001</b>
	C3 (R.U.)	0	0.06 ± 0.01	0.03 ± 0.01	<b>0.03 ± 0.02</b>	<b>0.05 ± 0.01</b>
	C4 (R.U.)	0.15 ± 0.02	<b>0.16 ± 0.02</b>	<b>0.17 ± 0.01</b>	<b>0.22 ± 0.001</b>	<b>0.20 ± 0.01</b>

Results after treatments ( $t = 5$  d) significantly different from the initial condition ( $t = 0$ ) at confidence level 0.05 are marked bold.

<sup>a</sup> SD standard deviation was calculated from the three replicate bottles.

by more than twofold, of up to 77% in winter flood tide (Fig. 7(c)). In addition, the broad range spanned by JDS samples along PC1 than XS samples (i.e., spanning from -3.69 to 4.95 for JDS samples on PC1 scores, compared to a small range between -2.32 and 3.08 of XS samples on this PC) may imply more variation in DOM source materials in JDS marsh than XS marsh. Taken together, PC1 appears to be associated with the dominant controls, for example, hydrology that drives the DOM source variabilities in the two marshes (Cawley et al., 2014; Chen et al., 2013; Osburn et al., 2015). On the contrary, on the second PC, regardless of tidal and seasonal shifts, JDS samples which were less humidified relative to XS marsh samples, mostly fall positively (ranging from 0.01 to 2.79) on this PC axis while most XS samples distribute on the negative scale (ranging between -3.46 and -0.01) of PC2. Therefore, despite the small variance (~16.9%) it accounts for, PC2 is likely indicative of the DOM quality differences or the state of degradation between the two study marshes (Shafiquzzaman et al., 2014; Yamashita et al., 2013).

Results in the PCA bi-plot also provide additional insight into the seasonal dynamics of marsh DOM quality. For example, most JDS summer and fall samples collected at ebb tide, which were predominately of terrestrial origin (high  $a_g(325)$  of  $5.27\ m^{-1}$  and high SUVA<sub>254</sub> of  $8.44\ L\ mg\ C^{-1}\ m^{-1}$ ) with less contribution from protein-like component C4 (11–19% to the total variance, Fig. 7(a)), and positively on the PC1 score, whereas the samples collected still at ebb tide but in winter-time, which is more enriched in C4 with contribution increasing approxi. to 40%, shift to the negative scale along PC1. Conversely, the nearly even distribution of ebb tide samples in XS marsh over the positive and negative scales on PC1, likely reflects the less variable DOM quality changes among seasons.

DOM changes as a result of the degradation processes are also clearly depicted by the PCA bi-plot. Light-exposed samples depleted with humic substances while enriched with proteinaceous materials occupy a different quadrant from the ones after the microbial treatment with minimal changes in the DOM quality on the first PC for both marshes

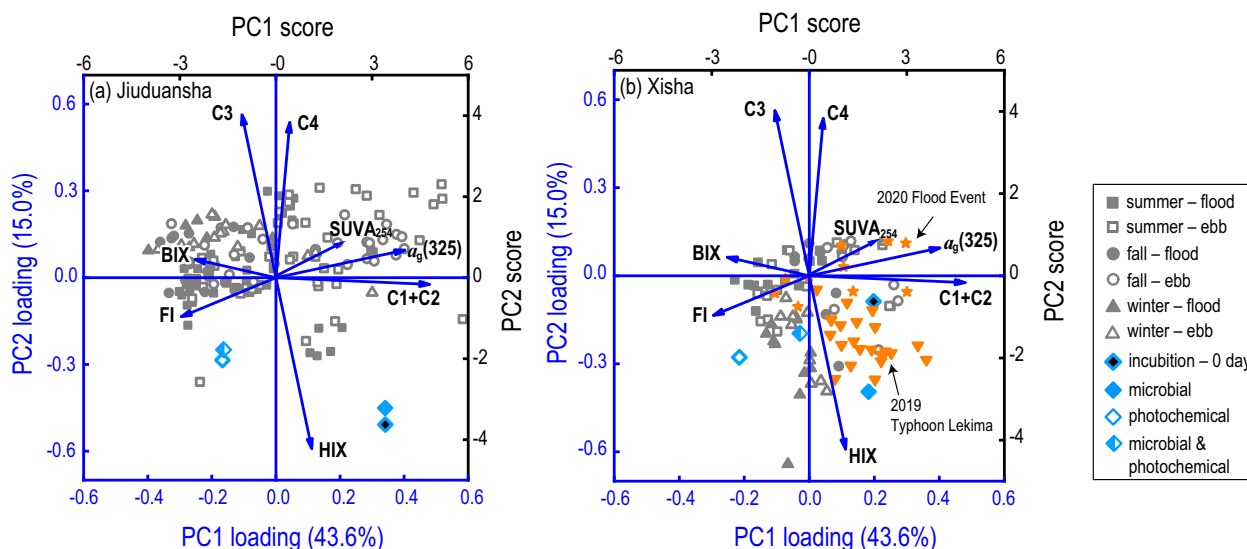
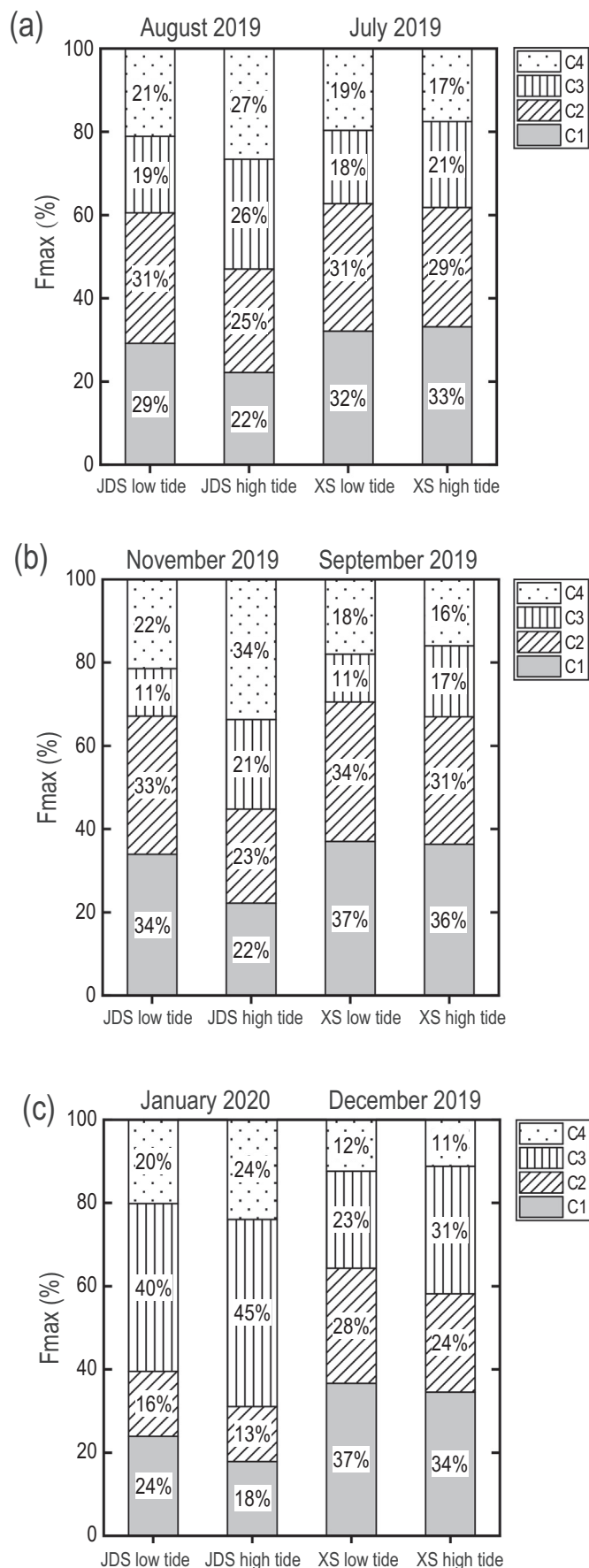


**Fig. 6.** The first two PCA loading and score of DOM optical properties from the JDS (a) and XS (b) marsh. C1 and C3 were merged because of the collinearity ( $R^2 = 0.92$ ).



(e.g., PC1 score = -1.67 and PC2 score = -2.03 for the light-exposure samples, relative to PC1 score = 3.41 and PC2 score = -3.21 for the microbial treated and PC1 score = 3.41 and PC2 score = -3.63 for the original samples, respectively, for JDS marsh DOM). These distributions of DOM degradation samples further substantiate our explanation of PC1 as an indicator of the dominant processes driving the DOM changes.

Grouping of samples into the fourth quadrant with positive scores on PC1 and negative scores on PC2 (ranging from 0.21 to 3.38 on PC1 and from -1.75 to -0.23 on PC2, respectively) correspond to most samples in the two episodic weather events, during which period the substantial export of terrestrial-derived OM was most pronounced. Yet, the 2020 summer Flood event samples are closely distributed while samples from the 2019 Typhoon event are slightly dispersed to the first and third quadrants, implying the DOM quality differences between these two extreme events.

It should be noted that the first two PCs capture roughly 60% of the total data variance. There is, however, still a substantial amount of variance (>40%) that has not been accounted for by PCA. This uncaptured variance emphasizes the temporal and spatial complexity, on both semidiurnal and seasonal scales, of the quantity and quality of DOM within and among the two marsh ecosystems, in which DOM dynamics can be influenced by processes other than seasonal and tidal shifts. On the other hand, this considerable amount of the uncaptured variance also likely arose from the high heterogeneity of the DOM across the two study marsh sites, warranting further work spanning more diverse hydrological regimes across the entire estuary to better assess the relative importance of physical and biogeochemical processes on coastal wetland DOM.

#### 4. Discussion

##### 4.1. Impact of large river on estuarine wetland DOM

The seasonal DOM dynamics across the tidal marsh-estuary margins in the CRE are strongly modulated by both the marsh productivity and the seasonal Changjiang runoff. High primary productivity in June to November marsh growing period and the coinciding monsoon-driven high runoff, gave rise to the seasonal peak DOC during both low and high tides. Conversely, the low Changjiang discharge in the wintertime during which marsh productivity was also lowest resulted in a seasonal minimal DOC.

In a river-dominated estuary, the influence of the fluvial-input terrestrial OM can be overwhelming such that the marsh signatures become less prominent (Letourneau and Medeiros, 2019). A good illustration is presented by the same percentage contribution of each FDOM component between JDS (salinity = 0.28 in low tide, August 2019) and XS (salinity = 0.16 in low tide, July 2019) study marshes at low tide in the wet season (Fig. 7(a)), highlighting the prevalence of the terrigenous OM associated with high riverine discharge throughout the entire estuary (Bittar et al., 2016; Dixon et al., 2014; Hounshell et al., 2021; Singh et al., 2019).

The importance of the runoff, particularly on the coastal tidal freshwater wetlands, is further underscored by the nearly identical proportional distribution of individual fluorescence components between the lowest ebb tide and highest flood tide in the summer-fall wet season (Fig. 7(a)). Moreover, the dominance of the proportional abundances of C1 and C2 (>60%) in total FDOM pools at the two different tidal stages in XS marsh in summer 2019 highlights the strong imprinting of terrigenous signatures in the FDOM pools resulting from the high Changjiang discharge. Recent studies have shown that DOM in Changjiang is primarily from the dissolved remnants of soil OM and the terrigenous

**Fig. 7.** The seasonal variations of the PARAFAC components proportions in JDS and XS marshes.

\*The L.T. and H.T. included the three data at the lowest depth and the highest depth in a tidal cycle, respectively.

DOM accounts for a higher fraction during the flood period (Bao et al., 2015; Ma et al., 2021). Therefore, these terrigenous DOM by fluvial inputs, largely comprised of humic substances (Gan et al., 2013; Guo et al., 2014), makes up a significant portion of the humic-like FDOM pools and results in an equivalent contribution of humic substances in the high tide relative to the low tide water (Fig. 7(a) and (b)). Furthermore, none of the five optical indices (i.e., SUVA<sub>254</sub>, S<sub>R</sub>, FI, BIX, and HIX) which are indicative of the OM sources and compositions has statistically significant differences between the high and the low tide for XS samples (Mann-Whitney *U* test,  $p > 0.05$ , Fig. 5(a)–(c) and Supplementary Table 1), highlighting the dominant riverine contribution to the FDOM pools in the coastal tidal freshwater wetlands.

However, despite the indistinguishable proportional contribution resulting from the prominent runoff, the fluorescence indices demonstrate significant differences among these samples (Fig. 7), suggesting the FDOM quality may likely be essentially different between these two coastal marshes. FI and HIX in the summer–fall low tide JDS marsh sample are statistically significantly lower than those from XS marsh (Mann-Whitney *U* test,  $p < 0.05$ ), reflecting the less humification in OM in JDS marsh. This may be attributed to the different landscape and salinity features between these two study marshes (see discussion below). Nevertheless, these results reflect the pervasive influence of large rivers such as Changjiang, on the estuarine wetland DOM dynamics.

#### 4.2. Factors contributing to DOM differences in the two marshes

The hydrological regimes exert substantial controls on coastal wetland DOM dynamics. The two study marshes reside along the estuarine salinity gradient, yet with distinct hydrological features. The XS marsh locates at the river end-member (salinity ~0) in the river-dominated South Branch of Changjiang with minimal oceanic exchange (Fig. 1(a)) (Chen et al., 1985). As such, this freshwater tidal wetland may likely have solely fluvial inputs by which soil erosion-sourced DOM dominated during flood tide (Bao et al., 2015), as supported by the unchanged humic components C1 and C2 on the tidal scale in Fig. 4(f) and by the decreased 6–10% of these two humic components in the wintertime when the runoff is lowest (Fig. 7(c)). Therefore, contributions from protein-like materials, which were likely be produced by the in-stream primary production with moderate or low discharge, accordingly increased as the humic proportion decreased (Ma et al., 2021; Wang et al., 2019). The JDS marsh, however, locates more seaward and is subject to strong hydrological exchanges with oceanic inputs from the adjacent East China Sea that is more enriched with autochthonous proteinaceous substances. Hence, during wintertime when marsh productivity and riverine runoff are both lowest, protein-like materials accounted for a predominant proportion in the FDOM pools (~70%), particularly during high tide in JDS marsh (Fig. 7(c)).

Differences in the landscape age can be also influential in shaping the different organic matter pools between the two marshes (Trumbore, 2000; Whittinghill and Hobbie, 2012). The JDS marsh is a newborn alluvial shoal of a much younger age than XS marsh (A. Gao et al., 2010). The lowest HIX (i.e., a value of 0.47) and higher BIX (i.e., a value of 1.0) in the low tide water in younger JDS marshland with less OM accumulation (Bradley-Cook and Virginia, 2015), most of which are presumably less degraded and largely labile (Darrouzet-Nardi, 2010), as evidenced by higher S<sub>R</sub> of 1.18 and low SUVA<sub>254</sub> of 5.74 L mg C<sup>-1</sup> m<sup>-1</sup>, are statistically different from those two fluorescence indices in XS marsh (Mann-Whitney *U* test,  $p < 0.05$ ). As a consequence, in wintertime when the microbes have a less dominant effect altering DOM under low ambient temperature, the less altered proteinaceous C4 contributes a substantial fraction of up to ~40% to the total fluorescence in JDS marsh (Fig. 7(c)). To compare, marsh soils in XS wetlands are much older which are likely associated with more degraded carbon of high aromaticity (with the highest SUVA<sub>254</sub> of 12.03 L mg C<sup>-1</sup> m<sup>-1</sup> and a high HIX of 0.67 during winter low tide, see Supplementary Table 1).

Sediment-derived DOM also potentially contributes to the DOM variability in the aquatic environment. Furthermore, in the winter dry season, samples collected during low tide in XS marsh show a dramatically increased SUVA<sub>254</sub> of 12.03 L mg C<sup>-1</sup> m<sup>-1</sup>, which was threefold higher relative to the summer flood season (i.e., SUVA<sub>254</sub> of 3.95 L mg C<sup>-1</sup> m<sup>-1</sup> at lowest ebb tide in July 2019). The winter DOM with a drastic elevation in SUVA<sub>254</sub>, accompanied with a decreasing S<sub>R</sub> to less than 1, may be attributed to the less intense photochemical degradation in winter (Frey et al., 2016; Weishaar et al., 2003). It may also likely be associated with the materials seeping through the sediments as sediment porewaters are reported to be more enriched with HMW high-aromaticity compounds (Chin et al., 1998; Clark et al., 2008; Lu et al., 2020; Schiebel et al., 2020).

## 5. Conclusions and implications

In the present study, we investigate the DOM characteristics in two coastal marshes along the Changjiang River Estuary. Variability of DOM was largely controlled by the tidal shifts on a short timescale and by the marsh seasonal cycle and the seasonal Changjiang runoff on a longer, seasonal timescale. Elevated levels in DOC concentration, CDOM absorption coefficient, and humic-like components were constantly found in the ebbing waters compared to the flood tide. On a seasonal basis, the highest values of these properties were found in the summer–fall time when the marsh productivity and riverine runoff both peak, while those values were lowest during the wintertime when the marsh was less productive and the runoff was also lowest during the year. Conversely, protein-like components in the two coastal marshes displayed a constant level regardless of the tidal and seasonal shifts. Our study also highlighted the predominance of photochemistry in altering marsh DOM across the marsh–estuary margins. PCA revealed the dynamics of DOM following the tidal and seasonal shifts and highlighted the influence of episodic extreme weather events on marsh DOM characteristics.

Our study also provides a unique comparison of DOM in two different coastal marshes along the CRE. Spatial and temporal heterogeneity in wetland DOM in the CRE is clearly noted between the two marshes as a result of different hydrological and landscape features. Therefore, upscaling or extrapolating the reported values in this study onto an estuary-wide ecosystem scale should be proceeded with caution. In addition, it appears challenging to distinguish the marsh-derived DOM from that derived from the fluvial systems in the terrigenous DOM pools by optical-based metrics, particularly in this study which Changjiang exerts a predominant control on the DOM compositions on the coastal wetlands. Nevertheless, results from this study highlight the preponderance of terrigenous OM by fluvial inputs delivered by large rivers on the coastal marsh DOM compositions and dynamics. Future efforts using more advanced molecular approaches including high-resolution mass spectroscopy should strive to distinguish marsh DOM from riverine DOM to better constrain DOM sources and fate across the river–coastal marsh–estuary continuum.

### CRedit authorship contribution statement

**Xiaohui Zhang:** Conceptualization, Data collection and analysis, Methodology, Writing – original draft & editing. **Fang Cao:** Conceptualization, Methodology, Data interpretation, Writing – original draft, review & editing. **Ying Huang:** Logistic support. **Jianwu Tang:** Conceptualization, Supervision, Funding acquisition, Writing – review, Responsible for the data product.

### Declaration of competing interest

The authors declare that they have no known competing financial interests or personal relationships that could have appeared to influence the work reported in this paper.

## Acknowledgment

This work was supported by grants from the Science and Technology Commission of Shanghai Municipality (#19230742300), and the “Ecology +” Initiative of the East China Normal University. We also acknowledge the support from the Chongxi Wetland Research Center, the Yangtze River Delta Estuary Wetland Station, and Shanghai Jiuduansha Wetland National Nature Reserve Administration for sampling and accommodation. Technical support by Ms. Ying Zhang and Ms. Minghui Du during the sampling periods are also gratefully acknowledged. We also thank the two anonymous reviewers for their detailed and constructive comments on this manuscript.

## Appendix A. Supplementary data

Supplementary data to this article can be found online at <https://doi.org/10.1016/j.scitotenv.2021.150993>.

## References

- Amon, R.M.W., Benner, R., 1996. Photochemical and microbial consumption of dissolved organic carbon and dissolved oxygen in the Amazon River system. *Geochim. Cosmochim. Acta* 60, 1783–1792.
- Arrigo, K.R., Brown, C.W., 1996. Impact of chromophoric dissolved organic matter on UV inhibition of primary productivity in the sea. *Mar. Ecol. Prog. Ser.* 140, 207–216.
- Bahram, M., Bro, R., Stedmon, C., Afkhami, A., 2006. Handling of rayleigh and raman scatter for PARAFAC modeling of fluorescence data using interpolation. *J. Chemom.* 20, 99–105.
- Bao, H., Wu, Y., Zhang, J., 2015. Spatial and temporal variation of dissolved organic matter in the Changjiang: fluvial transport and flux estimation. *J. Geophys. Res. Biogeosci.* 120, 1870–1886.
- Benner, R., 2002. Chemical composition and reactivity. In: Hansell, D.A., Carlson, C.A. (Eds.), *Biochemistry of Marine Dissolved Organic Matter*. Academic Press, San Diego, pp. 59–90.
- Bhattacharya, R., Osburn, C.L., 2020. Spatial patterns in dissolved organic matter composition controlled by watershed characteristics in a coastal river network: the Neuse River basin, USA. *Water Res.* 169, 115248.
- Bittar, T.B., Berger, S.A., Birs, L.M., Walters, T.L., Thompson, M.E., Spencer, R.G.M., et al., 2016. Seasonal dynamics of dissolved, particulate and microbial components of a tidal saltmarsh-dominated estuary under contrasting levels of freshwater discharge. *Estuarine Coastal and Shelf Science* 182, 72–85.
- Bradley-Cook, J.L., Virginia, R.A., 2015. Soil carbon storage, respiration potential, and organic matter quality across an age and climate gradient in southwestern Greenland. *Polar Biol.* 39, 1283–1295.
- Brym, A., Paerl, H.W., Montgomery, M.T., Handsel, L.T., Ziervogel, K., Osburn, C.L., 2014. Optical and chemical characterization of base-extracted particulate organic matter in coastal marine environments. *Mar. Chem.* 162, 96–113.
- Canuel, E.A., Cammer, S.S., McIntosh, H.A., Pondell, C.R., 2012. Climate change impacts on the organic carbon cycle at the land-ocean interface. *Annu. Rev. Earth Planet. Sci.* 40, 685–711.
- Cao, F., Medeiros, P.M., Miller, W.L., 2016. Optical characterization of dissolved organic matter in the Amazon River plume and the Adjacent Ocean: examining the relative role of mixing, photochemistry, and microbial alterations. *Mar. Chem.* 186, 178–188.
- Cawley, K.M., Yamashita, Y., Maie, N., Jaffé, R., 2014. Using optical properties to quantify fringe mangrove inputs to the dissolved organic matter (DOM) Pool in a subtropical estuary. *Estuar. Coasts* 37, 399–410.
- Chen, M., Jaffé, R., 2014. Photo- and bio-reactivity patterns of dissolved organic matter from biomass and soil leachates and surface waters in a subtropical wetland. *Water Res.* 61, 181–190.
- Chen, J., Zhu, H., Dong, Y., Sun, J., 1985. Development of the Changjiang estuary and its submerged delta. *Cont. Shelf Res.* 4, 47–56.
- Chen, M., Maie, N., Parish, K., Jaffé, R., 2013. Spatial and temporal variability of dissolved organic matter quantity and composition in an oligotrophic subtropical coastal wetland. *Biogeochemistry* 115, 167–183.
- Chin, Y.-P., Traina, S.J., Swank, C.R., Backhus, D., 1998. Abundance and properties of dissolved organic matter in pore waters of a freshwater wetland. *Limnol. Oceanogr.* 43, 1287–1296.
- Clark, C.D., Litz, L.P., Grant, S.B., 2008. Saltmarshes as a source of chromophoric dissolved organic matter (CDOM) to Southern California coastal waters. *Limnol. Oceanogr.* 53, 1923–1933.
- Clark, J.B., Neale, P., Tzortziou, M., Cao, F., Hood, R.R., 2019. A mechanistic model of photochemical transformation and degradation of colored dissolved organic matter. *Mar. Chem.* 214, 103666.
- Coble, P.G., 2007. Marine optical biogeochemistry: the chemistry of ocean color. *Chem. Rev.* 107, 402–418.
- Cory, R.M., Kaplan, L.A., 2012. Biological lability of streamwater fluorescent dissolved organic matter. *Limnol. Oceanogr.* 57, 1347–1360.
- Cory, R.M., McKnight, D.M., 2005. Fluorescence spectroscopy reveals ubiquitous presence of oxidized and reduced quinones in dissolved organic matter. *Environ. Sci. Technol.* 39, 8142–8149.
- Dai, S.B., Lu, X.X., 2014. Sediment load change in the Yangtze River (Changjiang): a review. *Geomorphology* 215, 60–73.
- Darrouzet-Nardi, A., 2010. Landscape heterogeneity of differently aged soil organic matter constituents at the Forest-Alpine Tundra Ecotone, Niwot Ridge, Colorado, U.S.A. *Arctic, Antarctic, and Alpine Research.* 42, pp. 179–187.
- Dixon, J.L., Osburn, C.L., Paerl, H.W., Peierls, B.L., 2014. Seasonal changes in estuarine dissolved organic matter due to variable flushing time and wind-driven mixing events. *Estuar. Coast. Shelf Sci.* 151, 210–220.
- Fagherazzi, S., Wiberg, P.L., Temmerman, S., Struyf, E., Zhao, Y., Raymond, P.A., 2013. Fluxes of water, sediments, and biogeochemical compounds in salt marshes. *Ecol. Process.* 2, 3.
- Fasching, C., Behounek, B., Singer, G.A., Battin, T.J., 2014. Microbial degradation of terrigenous dissolved organic matter and potential consequences for carbon cycling in brown-water streams. *Sci. Rep.* 4, 4981.
- Fellman, J.B., Hood, E., Spencer, R.G.M., 2010. Fluorescence spectroscopy opens new windows into dissolved organic matter dynamics in freshwater ecosystems: a review. *Limnol. Oceanogr.* 55, 2452–2462.
- Frey, K.E., Sobczak, W.V., Mann, P.J., Holmes, R.M., 2016. Optical properties and bioavailability of dissolved organic matter along a flow-path continuum from soil pore waters to the Kolyma River mainstem, East Siberia. 13, 2279–2290.
- Gan, X., Cai, Y., Choi, C., Ma, Z., Chen, J., Li, B., 2009. Potential impacts of invasive *Spartina alterniflora* on spring bird communities at Chongming Dongtan, a Chinese wetland of international importance. *Estuar. Coast. Shelf Sci.* 83, 211–218.
- Gan, S., Wu, Y., Bao, H., Zhang, J., 2013. Characterization of DOM (dissolved organic matter) in Yangtze River using 3-D fluorescence spectroscopy and parallel factor analysis (in Chinese with an English abstract). *China Environ. Sci.* 33, 1045–1052.
- Gao, A., Yang, S.L., Li, G., Li, P., Chen, S.L., 2010a. Long-term morphological evolution of a Tidal Island as affected by natural factors and human activities, the Yangtze Estuary. *J. Coast. Res.* 26, 123–131.
- Gao, K., Zhou, Z., Yang, Y., 2010b. Land use structure and its spatial autocorrelation analysis in the Yangtze River basin (in Chinese with an English abstract). 19, 13–20.
- Gao, L., Fan, D., Sun, C., Li, D., Cai, J., 2011. Optical characterization of CDOM in a marsh-influenced environment in the Changjiang (Yangtze River) estuary. *Environ. Earth Sci.* 64, 643–658.
- Gao, L., Gao, Y., Song, S., Zhang, F., 2020. Non-conservative behavior of dissolved organic carbon in the Changjiang (Yangtze River) Estuary and the adjacent East China Sea. *Cont. Shelf Res.* 197, 104084.
- Green, S.A., Blough, N.V., 1994. Optical absorption and fluorescence properties of chromophoric dissolved organic matter in natural waters. *Limnol. Oceanogr.* 39, 1903–1916.
- Guo, W., Yang, L., Zhai, W., Chen, W., Osburn, C., Huang, X., et al., 2014. Runoff-mediated seasonal oscillation in the dynamics of dissolved organic matter in different branches of a large bifurcated estuary—the Changjiang Estuary. *J. Geophys. Res. Biogeosci.* 119, 776–793.
- Hansell, D.A., Carlson, C.A., Repeta, D.J., Schlitzer, R., 2009. Dissolved organic matter in the ocean: a controversy stimulates new insight. *Oceanography* 22, 202–211.
- Harjung, A., Sabater, F., Butturini, A., 2018. Hydrological connectivity drives dissolved organic matter processing in an intermittent stream. *Limnologica* 68, 71–81.
- Hedges, J.L., 1992. Global biogeochemical cycles: progress and problems. *Mar. Chem.* 39, 67–93.
- Helms, J.R., Stubbins, A., Ritchie, J.D., Minor, E.C., Kieber, D.J., Mopper, K., 2008. Absorption spectral slopes and slope ratios as indicators of molecular weight, source, and photobleaching of chromophoric dissolved organic matter. *Limnol. Oceanogr.* 53, 955–969.
- Helms, J.R., Stubbins, A., Perdue, E.M., Green, N.W., Chen, H., Mopper, K., 2013. Photochemical bleaching of oceanic dissolved organic matter and its effect on absorption spectral slope and fluorescence. *Mar. Chem.* 155, 81–91.
- Herrmann, M., Najjar, R.G., Kemp, W.M., Alexander, R.B., Boyer, E.W., Cai, W.J., et al., 2015. Net ecosystem production and organic carbon balance of U.S. East Coast estuaries: a synthesis approach. *Glob. Biogeochem. Cycl.* 29, 96–111.
- Hosen, J.D., Armstrong, A.W., Palmer, M.A., 2018. Dissolved organic matter variations in coastal plain wetland watersheds: the integrated role of hydrological connectivity, land use, and seasonality. *Hydro. Process.* 32, 1664–1681.
- Hounshell, A.G., Fegley, S.R., Hall, N.S., Osburn, C.L., Paerl, H.W., 2021. Riverine discharge and phytoplankton biomass control dissolved and particulate organic matter dynamics over spatial and temporal scales in the Neuse River Estuary, North Carolina. *Estuar. Coasts*.
- Huguet, A., Vacher, L., Relexans, S., Saubusse, S., Froidefond, J.M., Parlanti, E., 2009. Properties of fluorescent dissolved organic matter in the Gironde Estuary. *Org. Geochem.* 40, 706–719.
- Jørgensen, L., Stedmon, C.A., Kragh, T., Markager, S., Middelboe, M., Søndergaard, M., 2011. Global trends in the fluorescence characteristics and distribution of marine dissolved organic matter. *Mar. Chem.* 126, 139–148.
- Lakowicz, J.R., 2006. *Protein fluorescence. Principles of Fluorescence Spectroscopy*. Springer, Boston, pp. 529–575.
- Letourneau, M.L., Medeiros, P.M., 2019. Dissolved organic matter composition in a marsh-dominated estuary: response to seasonal forcing and to the passage of a hurricane. *J. Geophys. Res. Biogeosci.* 124, 1545–1559.
- Letourneau, M.L., Schaefer, S.C., Chen, H., McKenna, A.M., Alber, M., Medeiros, P.M., 2021. Spatio-temporal changes in dissolved organic matter composition along the salinity gradient of a marsh-influenced estuarine complex. *Limnol. Oceanogr.* 66, 3040–3054.
- Li, X., Liu, J.P., Tian, B., 2016. Evolution of the Jiuduansha wetland and the impact of navigation works in the Yangtze estuary, China. 253, 328–339.
- Liu, D., Bai, Y., He, X., Chen, C.-T.A., Huang, T.-H., Pan, D., et al., 2020. Changes in riverine organic carbon input to the ocean from mainland China over the past 60 years. *Environ. Int.* 134, 105258.
- Logozzo, L., Tzortziou, M., Neale, P., Clark, J.B., 2021. 126, e2020JG005744.

- Lu, Y.H., Bauer, J.E., Canuel, E.A., Yamashita, Y., Chambers, R.M., Jaffe, R., 2013. Photochemical and microbial alteration of dissolved organic matter in temperate headwater streams associated with different land use. *J. Geophys. Res. Biogeosci.* 118, 566–580.
- Lu, Q., He, D., Pang, Y., Zhang, Y., He, C., Wang, Y., et al., 2020. Processing of dissolved organic matter from surface waters to sediment pore waters in a temperate coastal wetland. *Sci. Total Environ.* 742, 140491.
- Ma, Y., Mao, R., Li, S., 2021. Hydrological seasonality largely contributes to riverine dissolved organic matter chemical composition: insights from EEM-PARAFAC and optical indicators. *J. Hydrol.* 595, 125993.
- Mann, P.J., Davydova, A., Zimov, N., Spencer, R.G.M., Davydov, S., Bulygina, E., et al., 2012. Controls on the composition and lability of dissolved organic matter in Siberia's Kolyma River basin. *J. Geophys. Res. Biogeosci.* 117, G01028.
- McKnight, D.M., Boyer, E.W., Westerhoff, P.K., Doran, P.T., Kulbe, T., Andersen, D.T., 2001. Spectrofluorometric characterization of dissolved organic matter for indication of precursor organic material and aromaticity. *Limnol. Oceanogr.* 46, 38–48.
- Medeiros, P.M., Seidel, M., Ward, N.D., Carpenter, E.J., Gomes, H.R., Niggemann, J., et al., 2015. Fate of the Amazon River dissolved organic matter in the tropical Atlantic Ocean. *Glob. Biogeochem. Cycl.* 29, 677–690.
- Milliman, J.D., Farnsworth, K.L., 2011. Runoff, erosion, and delivery to the coastal ocean. *River Discharge to the Coastal Ocean: Runoff, erosion, and delivery to the coastal ocean.* Cambridge University Press, New York, pp. 13–69.
- Mobed, J.J., Hemmingsen, S.L., Autry, J.L., McGown, L.B., 1996. Fluorescence characterization of IHSS humic substances: total luminescence spectra with absorbance correction. *Environmental Science & Technology* 30, 3061–3065.
- Murphy, K.R., Stedmon, C.A., Waite, T.D., Ruiz, G.M., 2008. Distinguishing between terrestrial and autochthonous organic matter sources in marine environments using fluorescence spectroscopy. *Mar. Chem.* 108, 40–58.
- Murphy, K.R., Stedmon, C.A., Graeber, D., Bro, R., 2013. Fluorescence spectroscopy and multi-way techniques. *PARAFAC*, 5, 6557–6566.
- Ohno, T., 2002. Fluorescence inner-filtering correction for determining the humification index of dissolved organic matter. *Environ. Sci. Technol.* 36, 742–746.
- Osburn, C.L., Mikan, M.P., Etheridge, J.R., Burchell, M.R., Birgand, F., 2015. Seasonal variation in the quality of dissolved and particulate organic matter exchanged between a salt marsh and its adjacent estuary. *J. Geophys. Res. Biogeosci.* 120, 1430–1449.
- Osburn, C.L., Boyd, T.J., Montgomery, M.T., Bianchi, T.S., Coffin, R.B., Paerl, H.W., 2016. Optical proxies for terrestrial dissolved organic matter in estuaries and coastal waters. *Frontiers in Marine Science* 2, 127.
- Osburn, C.L., Oviedo-Vargas, D., Barnett, E., Dierick, D., Oberbauer, S.F., Genereux, D.P., 2018. Regional groundwater and storms are hydrologic controls on the quality and export of dissolved organic matter in two tropical rainforest streams, Costa Rica. *J. Geophys. Res. Biogeosci.* 123, 850–866.
- Panettieri, M., Guigue, J., Chemidlin Prevost-Bouré, N., Thévenot, M., Lévêque, J., Le Guillou, C., et al., 2020. Grassland-cropland rotation cycles in crop-livestock farming systems regulate priming effect potential in soils through modulation of microbial communities, composition of soil organic matter and abiotic soil properties. *Agric. Ecosyst. Environ.* 299, 106973.
- Pang, Y., Wang, K., Sun, Y., Zhou, Y., Yang, S., Li, Y., et al., 2021. Linking the unique molecular complexity of dissolved organic matter to flood period in the Yangtze River mainstream. *Sci. Total Environ.* 764, 142803.
- Peterson, B., Fry, B., Hullar, M., Saupe, S., Wright, R., 1994. The distribution and stable carbon isotopic composition of dissolved organic carbon in estuaries. *Estuaries* 17, 111–121.
- Rudolph, J.C., Arendt, C.A., Hounshell, A.G., Paerl, H.W., Osburn, C.L., 2020. Use of geospatial, hydrologic, and geochemical modeling to determine the influence of wetland-derived organic matter in coastal waters in response to extreme weather events. *Front. Mar. Sci.* 7, 1–18.
- Schiebel, H.N., Gardner, G.B., Wang, X., Peri, F., Chen, R.F., 2018. Seasonal export of dissolved organic matter from a New England salt marsh. *J. Coast. Res.* 34, 939–954.
- Schiebel, H.N., Peri, F., Chen, R.F., 2020. Dissolved organic matter export from surface sediments of a New England salt marsh. *Wetlands* 40 (4), 693–705.
- Seidel, M., Yager, P.L., Ward, N.D., Carpenter, E.J., Gomes, H.R., Krusche, A.V., et al., 2015. Molecular-level changes of dissolved organic matter along the Amazon River-to-ocean continuum. *Mar. Chem.* 177, 218–231.
- Shafiqzaman, M., Ahmed, A.T., Azam, M.S., Razzak, A., Askri, B., Hassan, H.F., et al., 2014. Identification and characterization of dissolved organic matter sources in Kushiro river impacted by a wetland. *Ecol. Eng.* 70, 459–464.
- Shang, P., Lu, Y., Du, Y., Jaffe, R., Findlay, R.H., Wynn, A., 2018. Climatic and watershed controls of dissolved organic matter variation in streams across a gradient of agricultural land use. *Sci. Total Environ.* 612, 1442–1453.
- Sholkovitz, E.R., 1976. Flocculation of dissolved organic and inorganic matter during the mixing of river water and seawater. *Geochim. Cosmochim. Acta* 40, 831–845.
- Siegel, D.A., Maritorena, S., Nelson, N.B., Hansell, D.A., Lorenzi-Kayser, M., 2002. Global distribution and dynamics of colored dissolved and detrital organic materials. *J. Geophys. Res. Oceans* 107 21-1–21-14.
- Singh, S., Dash, P., Sankar, M.S., Silwal, S., Lu, Y., Shang, P., et al., 2019. Hydrological and biogeochemical controls of seasonality in dissolved organic matter delivery to a Blackwater estuary. *Estuar. Coasts* 42, 439–454.
- Stedmon, C.A., Nelson, N.B., 2015. The optical properties of DOM in the ocean. In: Hansell, D.A., Carlson, C.A. (Eds.), *Biogeochemistry of Marine Dissolved Organic Matter*. Academic Press, Boston, pp. 481–508.
- Stepanaukas, R., Moran, M.A., Bergamaschi, B.A., Hollibaugh, J.T., 2005. Sources, bioavailability, and photoreactivity of dissolved organic carbon in the Sacramento-San Joaquin River Delta. *Biogeochemistry* 74 (2), 131–149.
- Tan, L.-S., Ge, Z.-M., Fei, B.-L., Xie, L.-N., Li, Y.-L., Li, S.-H., et al., 2020. The roles of vegetation, tide and sediment in the variability of carbon in the salt marsh dominated tidal creeks. *Estuar. Coast. Shelf Sci.* 239, 106752.
- Trumbore, S., 2000. Age of soil organic matter and soil respiration: radiocarbon constraints on belowground C dynamics. *Ecol. Appl.* 10, 399–411.
- Tzortziou, M., Neale, P.J., Osburn, C.L., Megonigal, J.P., Maie, N., Jaffe, R., 2008. Tidal marshes as a source of optically and chemically distinctive colored dissolved organic matter in the Chesapeake Bay. *Limnol. Oceanogr.* 53, 148–159.
- Tzortziou, M., Neale, P.J., Megonigal, J.P., Pow, C.L., Butterworth, M., 2011. Spatial gradients in dissolved carbon due to tidal marsh outwelling into a Chesapeake Bay estuary. *Mar. Ecol. Prog. Ser.* 426, 41–56.
- Wang, X.C., Chen, R.F., Gardner, G.B., 2004. Sources and transport of dissolved and particulate organic carbon in the Mississippi River estuary and adjacent coastal waters of the northern Gulf of Mexico. *Mar. Chem.* 89, 241–256.
- Wang, X., Ma, H., Li, R., Song, Z., Wu, J., 2012. Seasonal fluxes and source variation of organic carbon transported by two major Chinese Rivers: the Yellow River and Changjiang (Yangtze) River. 26.
- Wang, X., Wu, Y., Bao, H., Gan, S., Zhang, J., 2019. Sources, transport, and transformation of dissolved organic matter in a large river system: illustrated by the Changjiang River, China. 124, 3881–3901.
- Weishaar, J.L., Aiken, G.R., Bergamaschi, B.A., Fram, M.S., Fujii, R., Mopper, K., 2003. Evaluation of specific ultraviolet absorbance as an indicator of the chemical composition and reactivity of dissolved organic carbon. *Environ. Sci. Technol.* 37, 4702–4708.
- Whittinghill, K.A., Hobbie, S.E., 2012. Effects of pH and calcium on soil organic matter dynamics in Alaskan tundra. *Biogeochemistry* 111, 569–581.
- Yamashita, Y., Tanoue, E., 2003. Chemical characterization of protein-like fluorophores in DOM in relation to aromatic amino acids. *Mar. Chem.* 82, 255–271.
- Yamashita, Y., Kloeppel, B.D., Knoepf, J., Zausen, G.L., Jaffe, R., 2011. Effects of watershed history on dissolved organic matter characteristics in headwater streams. *Ecosystems* 14, 1110–1122.
- Yamashita, Y., Boyer, J.N., Jaffe, R., 2013. Evaluating the distribution of terrestrial dissolved organic matter in a complex coastal ecosystem using fluorescence spectroscopy. *Cont. Shelf Res.* 66, 136–144.
- Yang, S.L., Zhang, J., Zhu, J., Smith, J.P., Dai, S.B., Gao, A., et al., 2005. Impact of dams on Yangtze River sediment supply to the sea and delta intertidal wetland response. *J. Geophys. Res. Earth Surf.* 110, F03006.